TECHNICAL RESEARCH REPORT

Energy- and Power-Balance Assessment of Base Isolated
Structures Supplemented with Modified Bang-Bang Control

by Robert Sebastianelli, Mark Austin

SEIL TR 2005-2
(ISR TR 2005-90)

ISR Technical Report

Energy- and Power-Balance Assessment of

Base Isolated Structures Supplemented

with Modified Bang-Bang Control

By Robert R. Sebastianelli[1] and Mark Austin[2]

Last updated: May 4, 2005.

[1]Ph.D. Candidate, Department of Civil and Environmental Engineering, and Institute for Systems Research, University of Maryland, College Park, MD 20742, USA. E-mail : sebastn@isr.umd.edu

[2]Associate Professor, Department of Civil and Environmental Engineering, and Institute for Systems Research, University of Maryland, College Park, MD 20742, USA. E-mail : austin@isr.umd.edu

Contents

ABSTRACT

This report is the second in series investigating the feasibility of supplementing base isolation with active bang-bang control mechanisms. We formulate discrete approximations to energy- and power-balance equations for a base isolated structure supplemented with constant stiffness bang-bang (CKBB) control. Numerical experiments are conducted to: (1) Identify situations when constant stiffness bang-bang control is most likely to "add value" to system responses due to base isolation alone, and (2) Quantitatively determine the work done and power required by the actuators. A key observation from the numerical experiments is that "overall performance" of the actuators is coupled to "input energy per unit time."

0

Chapter 1

Introduction

1.1   Problem Statement

To assist engineers in the design of base isolated structures, recent AASHTO and UBC design codes [1, 52] contain code provisions prescribing a series of standard performance levels for design, together with acceptable levels of structural and non-structural damage, and suggested methods of analysis for performance evaluation. Under minor and moderate earthquake loadings, for example, base isolated structures should suffer no structural damage. For design earthquakes corresponding to the maximum credible ground motion for the site, the main structural members are expected to remain essentially elastic, with nonlinear deformations (i.e., damage) restricted to the isolation devices. Simplified methods of design for base isolated structures have been proposed by Turkington et al. [50, 49], Antriono and Carr [3, 2], Mayes et al. [31], and Ghobarah and Ali [17], among others. While these performance-based code provisions and simplified design procedures give high-level guidance regarding acceptable and unacceptable levels of performance (and how to achieve it), there is a mounting body of evidence that base isolation may not always provide adequate protection [60]. One concern is the possibility of localized buckling of the isolator devices and/or collapse of the structure caused by truly excessive lateral displacements of isolator elements (details on the appropriate analysis procedures can be found in Naeim and Kelly [32]). A second area of concern, raised by Johnson et al. [23] and Spencer et al. [44], points to the inability of base isolation to protect structures against near-source, high-velocity, long-period pulse earthquakes. In similar studies, Hall et al. [18] and Heaton et al. [19] express concerns about excessively large base drifts caused by strong, near-fault ground motions.

In a first step toward addressing these issues (and potentially achieving a higher level of performance), researchers have proposed systems where the main isolation devices are supplemented by active control mechanisms [39, 20]. Bang-bang control is a natural choice for the implementation of such a sys-

tem. While numerical algorithms exist for solving the Lyapunov matrix equation, systematic procedures for modeling base isolated structures, supplemented by bang-bang active control are still lacking [20]. Unresolved research questions include: What kinds of "performance improvement" are possible with active components? What are the limitations of present-day active component technologies? Answers to these questions are important because of their practical ramifications to design – base isolation alone is capable of reducing both the interstory drift and absolute accelerations structures at the expense of slight increases in base displacement. Looking ahead, we foresee base isolation supplemented by active control being able to achieve simultaneously low interstory displacements, low absolute accelerations, and controlled maximum base displacements [20, 44].

It is well known that use of overly complicated models too early in the design process can easily obscure interpretation of the underlying physical mechanisms and "cause-and-effect" relationships governing system performance. Hence, established design procedures use simplified models and analysis procedures for preliminary design (e.g., equivalent static lateral force procedures; linear elastic analysis procedures), where selection of the structural system, identification of desirable locations for inelastic actions, and tentative sizing of components are the primary problems, and then switch to high-fidelity models for validation of the final design [2, 55]. A framework of this type has not been developed for base isolated structures supplemented by active control. To help bridge this gap, we seek an analysis procedures that use performance-based metrics (e.g., displacements, velocities, energy) to capture the benefits of active control and base isolation, but are not overly complicated – indeed, we need to keep in mind that the complexity of the design method must be balanced against the uncertainty in ground motion prediction and in modeling of actual structural performance.

1.2 Objectives and Scope

This report is the second in series investigating the feasibility of supplementing base isolation with active control mechanisms, specifically bang-bang control. A key tenet of our work is that terms in the control design matrix (**Q**) should have well defined physical meaning, thereby opening a pathway for identifying and understanding basic cause-and-effect mechanisms that might exist in the implementation of passive/active base isolation systems. Wu, Soong, Gattulli, and Lin [58] suggest, for example, designing **Q** so that energy is minimized in the structure. With these goals in mind, the companion report [41] focuses on the formulation of simplified solutions to the Lyapunov equation that result from active control strategies driven by potential, kinetic and total energy concerns. A summary of key results and

required modeling assumptions can be found in Section 1.3. The beauty of simplified solutions is that they enable insight into cause-and-effect mechanisms existing between the underlying "mechanisms and parameters of bang-bang control" and "resulting behavior for various classes of structural system." The parameters of bang-bang control include structural properties (i.e., mass, damping, and stiffness matrices). The mechanisms bang-bang control include the direction of the actuator force as controlled by the system displacements and velocities. Numerical experiments were conducted to verify the predictions made during the analytical phase of the study.

In this study, we formulate energy- and power-balance equations for a base isolated structure supplemented with constant stiffness bang-bang (CKBB) control. CKBB control is discussed in detail in Section 1.3. While quantitative measurements such as absolute roof acceleration are a good indicator of damage to light internal equipment, occupant discomfort, and other non-structural damage [24], energy- and power-balanced based metrics of system performance provide a means for accurately estimating the capacity of a structure to resist forces elastically and dissipate energy associated with damping and key structural elements undergoing cyclic nonlinear deformations. In addition, because the objective of constant stiffness bang-bang (CKBB) control is motivated by minimum energy concerns, analyzing the system response from an energy/power point of view will help us to validate the theoretical formulation for CKBB control.

For the numerical experiments, we employ modeling techniques and a base isolated building structure assembled from a variety of previous research efforts. On the modeling front, there are two possible coordinate frames (moving- and fixed-base coordinates) to base our derivation – in this study, we only use the fixed-base (or relative) system. This derivation is as presented in Austin and Lin [5]. Nonlinear time-history analyses with energy- and power-balance assessment are computed for a 6-DOF base isolated building system. The parameters of the model are the same as used by Ramallo et al. [38]. (In turn, properties of the superstructure model reported by Ramallo et al. [38] are guided by a five-story building model given by Kelly et al. [25].) With this computational framework in place, the specific research objectives of this study are as follows:

1. From an energy- and power-balance viewpoint, compare the performance of a base isolated building subjected to a variety of design criteria and earthquakes.

2. Compare demands on actuator power to the capabilities of actuator technology.

Experimental permutations in the design and ground motion excitations include: (1) Base isolation alone

3

(with no control); (2) Base isolation supplemented by suboptimal bang-bang control; (3) Moderate earthquakes; (4) Near-source, high-velocity, severe earthquakes. We demonstrate that when the model parameters/behavior do not satisfy the assumptions needed to derive simplified representations for active control, it seems that good performance can still result. We say "it seems" because our modeling assumptions represent control under a "best case" scenario. As we move toward modeling of full-scale structures, several modeling assumptions would need to be reexamined: (1) Is a singular control-force requirement really possible?, (2) Availability of state variables (i.e., displacements and velocities at all DOFs), (3) No time delay between the measured displacements and velocities and the application of the control forces, and (4) The presence of only one actuator that is located at the top of the base isolator.

1.3   Constant Stiffness Bang-Bang (CKBB) Control

The effect of suboptimal bang-bang control on the second-order differential equation of motion for a seismically-resistant structure is as follows:

$$\mathbf{M}\ddot{x}(t) + \mathbf{C}\dot{x}(t) + \mathbf{K}x(t) = -\mathbf{H}u_{max}\text{sgn}\left[\mathbf{B^T S}\left(\begin{array}{c} x(t) \\ \dot{x}(t) \end{array}\right)\right] - \mathbf{M}r\ddot{x}_g(t); \tag{1.1}$$

where the matrix, $\mathbf{S}$, is the $2n$ x $2n$ matrix solution to the Lyapunov matrix equation given in the following equation:

$$\mathbf{A^T S} + \mathbf{S A} = -\mathbf{Q}. \tag{1.2}$$

and $\mathbf{B}$ is a $2n$ x p matrix given by:

$$\mathbf{B} = \left[\begin{array}{c} \mathbf{0} \\ \mathbf{M^{-1} H} \end{array}\right]. \tag{1.3}$$

Recent research suggests that overall input energy needs to be partitioned into two parts: (1) energy directed to the main structural system, and (2) energy directed to the base isolated devices [5, 8, 9, 48]. For the cases of partitioned input energies, a methodology for calculating $\mathbf{Q}$ has recently been developed by Sebastianelli and Austin [41]. Unfortunately, the symbolic expressions are lengthy and not scalable to systems beyond two-degrees of freedom. However, the solution to the Lyapunov equation greatly simplifies when the structure has uniform mass (i.e., $m_1 = m_2 = \ldots = m_n$), damping is in the form $\alpha \cdot \mathbf{M} + \beta \cdot \mathbf{K}$ is [41], and the design objective is minimization of overall potential energy:

4

$$\mathbf{B^T S} = \left[\begin{array}{cc} \frac{\mathbf{H^T}}{2} & \frac{\mathbf{H^T M}(\alpha \cdot \mathbf{M} + \beta \cdot \mathbf{K})^{-1}}{2} \end{array} \right];$$ (1.4)

When the acronym CKBB control is used, the "constant stiffness" portion refers to whether $\mathbf{B^T S}$ numerically varies when elastic and inelastic states are encountered when calculating the time history or $\mathbf{B^T S}$ is calculated based only on the elastic stiffness of the base isolator. Sebastianelli and Austin [41] showed that bang-bang control is insensitive to the nonlinearity of base isolators, and that an elastic or "constant" stiffness may be used to calculate $\mathbf{B^T S}$. Numerically, $\mathbf{B^T S}$ may be calculated using one of two equations: if the masses in the structure are uniform and damping is present in the form $\alpha \cdot \mathbf{M} + \beta \cdot \mathbf{K}$, using equation 1.4 or for all other cases, the Lyapunov equation (1.2) must be solved for $\mathbf{S}$ and pre-multiplied by $\mathbf{B^T}$.

Questions such as the following remain unanswered: Under what ground motion conditions is it beneficial to supplement based isolation with active control? What is the interaction between design of the superstructure, base isolator(s), and active control components? When is it beneficial to start/stop active control when the time history of the structure? What are the technology limitations of actuators?

Chapter 2

Energy- and Power-Balance Analysis

2.1 Background

Ideas in energy-based design date back to Housner [21, 22] in the 1950s, and have recently been revised by a number of researchers, including Powell and Allahabadi [37], Fajfar [16], and Bertero and co-workers [51, 56]. Generally speaking, these papers fall into three categories: (1) proposals for empirical design methods based upon energy ideas, (2) uses of energy in the performance assessment of energy dissipation devices and/or structural system configurations, and (3) analytical procedures for energy-balance calculations. As a result of this work, it is now understood that use of energy concepts provides:

1. A theoretical framework for connecting estimates of seismic input energy to spatial and temporal distributions of energy demand on structural subsystems and elements. The energy capacity of a structure is represented by the elastic capacity plus energy dissipation capacity associated with damping and key structural elements undergoing cyclic nonlinear deformations.

2. A rational means for accurately estimating the capacity of a structure. For example, it is now widely recognized that levels of damage caused by earthquakes do not depend on peak displacements alone. Instead, the cumulative damage from numerous inelastic cycles should be taken into account [16, 37].

The use of energy concepts in seismic design and analysis is appealing because very complex spatial and temporal distributions of linear/nonlinear deformations can be represented by mathematical scalars (i.e., simple mathematical models). From a numerical analysis viewpoint, an energy balance check provides a means of validating the computations are stable and accurate.

6

2.2 Equation of Motion

The left-hand side of Figure 2.1 shows the coordinate scheme for dynamics of a multi-degree of freedom structure subject to a horizontal time-varying base motion (actuators not shown). With respect to an absolute coordinate scheme, the equations of equilibrium may be written as a family of n 2nd order differential equations:

$$\mathbf{M}\ddot{x}_t(t) + \mathbf{F}(\dot{x}(t), x(t)) = \mathbf{H}u(t) \tag{2.1}$$

with initial conditions $x_t(0)$ and $\dot{x}_t(0)$. Here $x_t(t) = [x_{1t}(t), x_{2t}(t) ... x_{nt}(t)]^T$ is a $(n \times 1)$ vector of *absolute* system displacements, $\mathbf{M}$ is a $(n \times n)$ mass matrix, and $\mathbf{F}(\dot{x}(t), x(t))$ is a $(n \times 1)$ vector of straining and damping forces depending on displacements and velocities measured *relative* to the base motion. In other words, $\mathbf{F}(\dot{x}(t), x(t)) = \mathbf{F}_{\text{damping}}(\dot{x}(t), x(t)) + \mathbf{F}_{\text{straining}}(\dot{x}(t), x(t))$. $\mathbf{H}$ is an $n \times p$ matrix that designates the location of the controller(s), while $u(t)$ is a p-dimensional vector that represents the control force of p-number of controllers. For many engineering applications, the straining force is obtained directly from the stress-strain curve and the damping force is given by

$$\mathbf{F}_{\text{damping}}(\dot{x}(t), x(t)) = \mathbf{C}\dot{x}(t) \tag{2.2}$$

where $\mathbf{C}$ is a matrix of coefficients for linear viscous damping. The relationship between absolute and relative displacements is simply given by:

$$x_t(t) = x(t) + rx_g(t) \tag{2.3}$$

where $x_g(t)$ is the horizontal ground displacement and $\mathbf{r}$ is a $(n \times 1)$ vector describing the movement in each of the structural degrees of freedom due to a unit ground displacement, Substituting equation 2.3 into 2.1 and rearranging terms gives:

$$\mathbf{M}\ddot{x}(t) + \mathbf{F}(\dot{x}(t), x(t)) = \mathbf{H}u(t) - \mathbf{M}r\ddot{x}_g(t) \tag{2.4}$$

The right-hand side of Equation 2.4 is a vector of equivalent external loads applied at the nodal degrees of freedom caused by the earthquake ground motions plus, actuator forces applied to the external degrees of freedom. As before, $\ddot{x}_g(t)$ is the ground acceleration at time t.
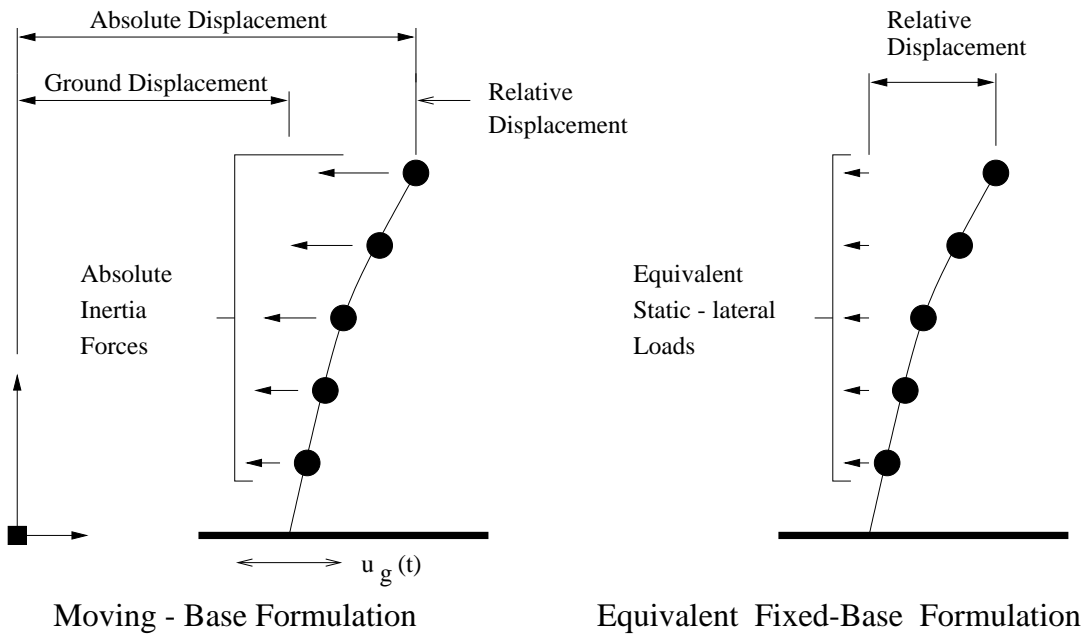
Figure 2.1: Moving- and Equivalent-base Models of System Response (forces due to active control not shown)

In moving from equations 2.1 to 2.4 we are removing the effects of rigid-body displacements from the problem formulation. From a computational standpoint, this is desirable because matrix equations 2.4 may be written entirely in terms of relative displacements (and ground displacements).

2.3 Formulation of Energy-Balance Equations

Let $\mathbf{R}(\dot{x}(\tau), x(\tau))$ be a force that depends on displacements $x(\tau)$ and velocities $\dot{x}(\tau)$. The work done by $\mathbf{R}(\cdots)$ over the time interval $\tau \in [0, t]$ is denoted $W(t)$, and is given by:

$$\text{W(t)} = \int_0^t \dot{x}^T(\tau) \cdot \mathbf{R}(\dot{x}(\tau), x(\tau))d\tau \tag{2.5}$$

At the highest level of abstraction the energy balance equations can be written:

$$\mathbf{W}_{\text{int}}(t) + \mathbf{T}(t) = \mathbf{W}_{\text{act}}(t) + \mathbf{W}_{\text{eq}}(t) = \mathbf{W}_{\text{ext}}(t), \tag{2.6}$$

where $\mathbf{W}$, without subscripts, represents work done and $\mathbf{T}$ represents kinetic energy. Equation 2.6 states that the work done by external loads/forces is converted to kinetic energy and/or internal energy. In this section we derive energy balance equations for (1) the moving base formulation, and (2) the equivalent fixed-base formulation. Energy balance equations have been formulated by Austin and Lin [5] in both

8

the moving- and fixed-base coordinate frames. These energy balance equations are modified to account for the work done by the active control and used in energy-balance assessment.

2.3.1 Energy Balance Equations for Equivalent Fixed-Based (or Relative) System

Substituting equation 2.1 into 2.5 and rearranging terms gives:

$$\int_0^t \dot{x}^T(\tau)\mathbf{M}\ddot{x}(\tau)d\tau + \int_0^t \dot{x}^T(\tau)\mathbf{F}(\dot{x}(\tau), x(\tau))d\tau = \int_0^t \dot{x}^T(\tau)\mathbf{H}u(\tau)d\tau - \int_0^t \dot{x}^T(\tau)\mathbf{M}r\ddot{x}_g(\tau)d\tau \quad (2.7)$$

The left-most term represents the work done by nodal inertia forces. The second term represents the work done by internal forces – due to condensation of boundary nodes, internal energy can be expressed in terms of relative displacements and velocities alone. The first term on the right-hand side represents the work done by the actuator forces $\mathbf{H}u(t)$ moving through relative displacements $x(t)$. The right-most term represents work done by equivalent static lateral nodal forces -$\mathbf{M}r\ddot{x}_g(t)$ moving through relative displacements $x(t)$. Integrating the left-most term by parts gives the kinetic energy, $\mathbf{T}(x(t))$, associated with relative displacements alone–it equals the integral of work done by equivalent static lateral node forces over the time interval $[0, t]$.

2.4 Discrete Approximation for Energy Balance Equations

Discrete approximation of the energy balance equations is necessary when they are being used in a interactive, time-step analysis. Discrete approximation of the energy balance equations for only the fixed-base (or relative) coordinate frame is considered here.

The internal work, $\mathbf{W}_{\text{int}}(t + \Delta t)$, represents the work done by the internal nodal forces moving through the degree of freedom displacements, and is given by

$$\mathbf{W}_{\text{int}}(t + \Delta t) = \mathbf{W}_{\text{int}}(t) + \int_t^{(t+\Delta t)} \dot{\mathbf{W}}_{\text{int}}(\tau)d\tau. \quad (2.8)$$

For damped systems, internal nodal forces, $\mathbf{F}_{\text{int}}$, are the sum of damping and straining force components. The rate of internal work is given by:

$$\dot{\mathbf{W}}_{\text{int}}(t) = \dot{x}(t)^T\mathbf{F}_{\text{int}}(t) = \dot{x}(t)^T\left[\mathbf{F}_{\text{straining}}(t) + \mathbf{F}_{\text{damping}}(t)\right]. \quad (2.9)$$

Substituting 2.9 into 2.8 and approximating the integral by the trapezoidal rule gives

9

$$\mathbf{W}_{\text{int}}(t + \Delta t) = \mathbf{W}_{\text{int}}(t) + \frac{\Delta t}{2}(\dot{x}(t)^T \mathbf{F}_{\text{int}}(t) + \dot{x}(t + \Delta t)^T \mathbf{F}_{\text{int}}(t + \Delta t)). \tag{2.10}$$

The work done by externally applied nodal loads is given by

$$\mathbf{W}_{\text{ext}}(t + \Delta t) = \mathbf{W}_{\text{ext}}(t) + \int_t^{(t+\Delta t)} \dot{\mathbf{W}}_{\text{ext}}(\tau) d\tau. \tag{2.11}$$

For the equivalent fixed-base formulation, the rate of work done by earthquake loads is $\dot{W}_{\text{eq}}(t) = -\dot{x}^T(t)\mathbf{M}r\ddot{u}_g(t)$. Approximating equation 2.11 by the trapezoidal rule gives

$$\mathbf{W}_{\text{eq}}(t + \Delta t) = \mathbf{W}_{\text{eq}}(t) + -\frac{\Delta t}{2}(\dot{x}(t)^T \mathbf{M}r\ddot{x}_g(t) + \dot{x}(t + \Delta t)^T \mathbf{M}r\ddot{x}_g(t + \Delta t)). \tag{2.12}$$

Similarly, the rate of work done by actuator forces is $\dot{W}_{\text{act}}(t) = \dot{x}^T(t)\mathbf{H}u(t)$. Approximating equation 2.11 by the trapezoidal rule gives

$$\mathbf{W}_{\text{act}}(t + \Delta t) = \mathbf{W}_{\text{act}}(t) + \frac{\Delta t}{2}(\dot{x}(t)^T \mathbf{H}u(t) + \dot{x}(t + \Delta t)^T \mathbf{H}u(t + \Delta t)). \tag{2.13}$$

The kinetic energy at time t is given by:

$$\int_0^t \dot{x}^T(\tau)\mathbf{M}\ddot{x}(\tau) d\tau = \frac{1}{2}\left[\dot{x}^T(\tau)\mathbf{M}\dot{x}(\tau)\right]_0^t = \mathbf{T}(\dot{x}(t)). \tag{2.14}$$

Chapter 3

Numerical Experiments

3.1 Objectives and Scope

For a wide range of moderate-to-large ground motion events, base isolated structures are expected to exhibit nonlinear displacement behavior at the isolator level, leaving the main structural system undamaged. While quantitative measurements such as peak values of velocity are a good indicator of non-structural damage [24], energy- and power-balance metrics of system performance provide a means for accurately estimating the capacity of a structure to resist forces elastically and dissipate energy associated with damping and key structural elements undergoing cyclic nonlinear deformations. Accordingly, in this chapter we exercise the theoretical framework for energy- and power-balance analysis by computing the time-history response of a six-DOF nonlinear mass-spring-damper system subject to an ensemble of moderate and severe ground excitations, plus constant stiffness bang-bang (CKBB) control. The purposes of the numerical experiment are three-fold:

1. To calculate the work done by the base isolators, superstructure, and actuators,

2. To assess the ability of present-day actuator technologies to deliver actuator power requirements estimated through simulation, and

3. To identify and quantitatively evaluate situations (e.g., moderate versus severe earthquake; expected versus unexpected ground motions) when CKBB control has the potential for adding significant value to overall performance, compared to base isolation alone.

Item 3 can be derived, in part, from the first two objectives and time histories of base drift. The scope of this study is restricted to constant stiffness bang-bang (CKBB) control; this decision is enabled by findings in the companion study [41].
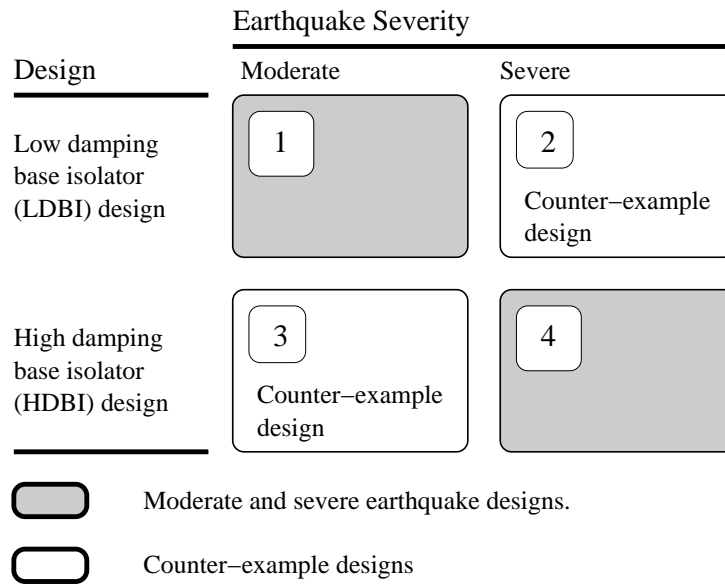
Figure 3.1: Scope of Case Study and Counter-Example Designs covered by the Numerical Experiments

The numerical experiment covers the range of design cases shown in Figure 3.1. The shaded boxes show the two case-study designs: (1) A low damping base isolation (LDBI) system designed to withstand ground motions of moderate intensity, and (2) A high damping base isolation (HDBI) system designed to withstand ground motions of severe intensity. Details of the LDBI and HDBI design procedures will be explained in Section 3.2.1. The unfilled boxes show the two design counter-examples: (1) The LDBI system is subject to a severe earthquake, and (2) The HDBI system is subject to a moderate earthquake. The purpose of the counter examples is to see how CKBB control works seismic events on an unexpected size occur. To quantify improvements in performance due to control, the actively controlled time history responses are benchmarked against corresponding LDBI/HDBI systems responses for base isolation alone. All numerical computations are implemented with the Aladdin scripting language [6, 7].

3.2 Properties of the Actively Controlled Base Isolated Structure

Figure 3.2 shows an elevation view of the six-DOF idealized mass-spring-damper model (This model has previously been employed by Ramallo et al. [38], which in turn can be traced to a five-story building model used by Kelly et al. [25].) Tables 3.1 and 3.2 summarize the structural parameters for the low damping base isolator (LDBI) design. For both the LDBI and HDBI designs the mass and damping properties are as shown in Table 3.1. Table 3.3 summarizes the structural parameters for the high damping base isolator (HDBI) design. Boundary conditions for the model are full-fixity at the base and full-fixity against vertical displacements and rotations at nodes 2 through 6.
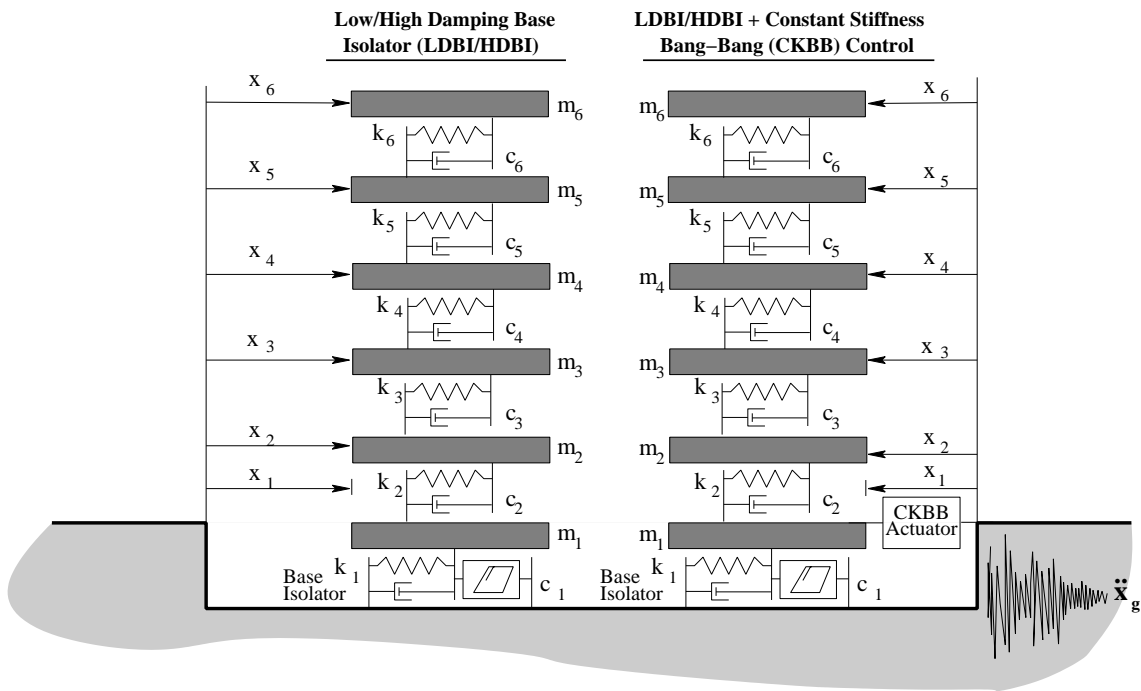
Figure 3.2: Elevation View of 6 DOF Linear/Nonlinear Mass-Spring-Damper System

	Floor	Damping	Stiffness (kN/m)	
DOF/Mode	Mass (kg)	(kN·s/m)	Pre-yield	Post-yield
1	6,800	3.74	1,392	232
2	5,897	67	33,732	33,732
3	5,897	58	29,093	29,093
4	5,897	57	28,621	28,621
5	5,897	50	24,954	24,954
6	5,897	38	19,059	19,059

Table 3.1: Mass, Damping and Stiffness Properties of Six-DOF Mass-Spring-Damper Model with Low Damping Base Isolator (LDBI)

	Period (secs)		Part. Factor (Γ)	
DOF/Mode	Pre-yield	Post-yield	Pre-yield	Post-yield
1	1.05	2.50	1.05	1.01
2	0.18	0.18	0.06	0.01
3	0.10	0.10	0.01	0.00
4	0.07	0.07	0.01	0.00
5	0.05	0.05	0.00	0.00
6	0.05	0.05	0.00	0.00

Table 3.2: Natural Periods of Vibration and Modal Participation Factors for Six-DOF Mass-Spring-Damper Model: with Low Damping Base Isolator (LDBI)

	Stiffness (kN/m)		Period (secs)		Part. Factor (Γ)	
DOF/Mode	Pre-yield	Post-yield	Pre-yield	Post-yield	Pre-yield	Post-yield
1	2,320	232	0.83	2.50	1.08	1.01
2	33,732	33,732	0.18	0.18	0.09	0.01
3	29,093	29,093	0.10	0.10	0.02	0.00
4	28,621	28,621	0.07	0.07	0.01	0.00
5	24,954	24,954	0.05	0.05	0.01	0.00
6	19,059	19,059	0.05	0.05	0.00	0.00

Table 3.3: Properties of Six DOF Mass-Spring-Damper Model with High Damping Base Isolator (HDBI)

The base isolation element is modeled as a bilinear solid with a force-displacement relationship that follows the kinematic hardening rule. This element was used by Lin [28] and is a model of a laminated rubber isolator with a lead core. The initial and post-yield shear stiffnesses of the isolator are $K_{initial}$ and K_{yield}, respectively. The latter is generated by the stiffness of the rubber, and is fixed at ($K_{yield} = 232$kN/m), as to give a post-yield period of 2.5 seconds. Pre-yield to post-yield ratios, and the isolator yield force (F_y) are left as design parameters; the design details will be covered in Section 3.2.1. The scope of this study is restricted to two values that give good performance for both moderate and severe ground motions. Viscous damping from the rubber is assumed to be 2% critical damping.

For the case of base isolation plus constant stiffness bang-bang (CKBB) control, the base isolation (BI) mechanism is supplemented by a controllable actuator that switches from one extreme to another (i.e., the control force is always exerting its maximum force in either the positive or negative direction). Solutions to the CKBB control problem are based on energy-inspired formulations of the Lyapunov equation, the details of which may be found in the companion paper by Sebastianelli and Austin [41].

3.2.1 Base Isolator (BI) Design

Ramallo et al. [38] considers two parameters in the design of the BI, the total yield force, F_y, which is expressed as a fraction of the total structural weight, and the pre-yield to post-yield stiffness ratio of the LRB, $K_{initial}/K_{yield}$. To obtain a post-yield fundamental period of 2.5 seconds, the post-yield stiffness is fixed at $K_{yield} = 232$ kN/m. The research supporting the low- and high-damping base isolator design procedures is as follows:

1. **Low Damping Base Isolator (LDBI).** Skinner et al. [42] suggest that for earthquakes having the "severity and character" of El Centro, typical values of the yield force (F_y) should be around 5% of the total structural weight. Park and Otsuka [34] recommend that F_y range from 4.3 to 5% of

14

the total structural weight for moderate earthquakes (peak ground acceleration (PGA) of 0.35g). In a third study by Ramallo et al. [38], plots of base drift and structural acceleration as a function of F_y for several values of the stiffness ratio, $K_{initial}/K_{yield}$ were constructed for two- and six-DOF models. The latter study suggests that in order to obtain moderate base drift and acceleration reduction for a ground excitation with PGA=0.35g, use $F_y = 5\%$ of the total structural weight and $K_{initial}/K_{yield} = 6$. This low damping base isolation system falls into the "Class (ii): lightly damped" category of Skinner et al. [42].

2. **High Damping Base Isolator (HDBI).** For severe earthquake events, such as the Kobe and Northridge earthquakes, Ramallo et al. [38] found that in order to obtain significant reductions in base drift and moderate accelerations, BI yield strengths and stiffness ratios need to be increased (relative to optimal values for moderate ground motions). Similar observations are reported by Park and Otsuka [34]. They found that for severe ground motion attacks (i.e., PGA of 1.225g), system performance is best when F_y in the range 14 to 18% of total structural weight.

Hence, in this study, the low damping base isolation (LDBI) design has $F_y = 14.46$ kN (which is 5% of the building weight) and $K_{initial}/K_{yield} = 6$. As noted by Ramallo et al. [38], the LDBI design is typical of low damping isolation systems used in engineering practice, is readily attainable using current technology, and follows standard AASHTO code procedures [1]. The high damping base isolator (HDBI) design has a yield force of $F_y = 43.39$ kN = 15% of the building weight and a stiffness ratio of $K_{initial}/K_{yield} = 10$. HDBI designs are not widely used in practice at this time. This may change, however, since there is now significant concern [18, 19, 44] that base isolated buildings may not be able to accommodate severe near-fault earthquakes.

3.2.2   Actuator Placement and Performance

This section describes issues associated with actuator placement and performance (i.e., actuator force/reach and on/off characteristics).

Actuator Placement. Housner et al. [20] and Reinhorn et al. [39] indicate that a key potential benefit in supplementing passive base isolated structures with active control is the possibility of simultaneously achieving (with a single set of control forces) low interstory drifts and limited maximum base displacements. Hence, the scope of this study will be restrictced to effects of CKBB control for a single actuator positioned at the top of the base isolator (i.e., at degree of freedom 1).

15
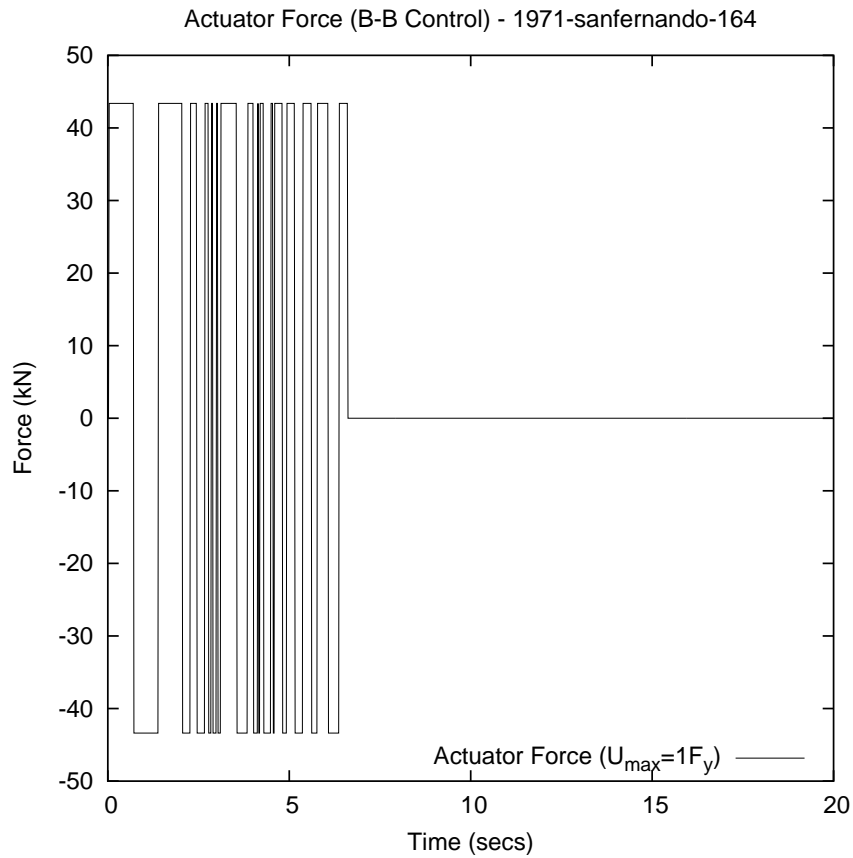
Figure 3.3: Actuator Time History Subjected to 1971 San Fernando

Duration of Performance. A key goal of this study is to mitigate a severe limitation of standard time-history analyses, exposed in the companion paper by Sebastianelli and Austin [41]. The companion study showed that at the end of the time-history analyses, often the top of the base isolator oscillates around a zero displacement and the actuator force switches between $\pm u_{max} = 350$ kN at a high frequency. This behavior adds very little value in terms of reduced displacements. To complicate matters (near the end of the ground excitation), the actuator can drive the system response by injecting mechanical energy into the structural system. Injection of mechanical energy has the potential of destabalizing the system in a bounded (input/output) sense.

Clearly, in the long term we need a systematic strategy for turning the actuator system on, and at some point later in time, turning it off. Because Arias Intensity accounts for overall energy characteristics of the accelerogram, as a first step in this direction, in this study we will use this parameter to limit the duration for which the actuator is on. When the Arias Intensity for a particular accelerogram reaches 90% of its constrained value (1.29 m/sec and 10.86 m/sec for moderate and severe earthquakes, respec-

16

tively), the actuator will be turned off. Figure 3.3 shows, for example, the time history of actuator force corresponding to the high damping system response generated by the 1971 San Fernando earthquake. The 1971 San Fernando earthquake reaches an Arias Intensity of 10.86 m/sec 6.62 seconds into the time history. A complete discussion of simulation scenarios will be given in Section 3.4.

Magnitude of Actuator Force. In order to provide for a fair comparison between the performance of passive BI damping mechanisms and hybrid LDBI/HDBI+CKBB damping mechanisms, the maximum actuator force (u_{max}) is treated as a design variable. We proceed under the assumption that the LDBI/HDBI+CKBB will not add value to the overall system performance unless the passive and active damping components can work in concert. Skinner et al. [42], Wang and Liu [57], Park and Otsuka [34], and Ramallo et al. [38] have shown that LDBI and HDBI perform well for moderate and servere ground excitations with yield forces, F_y, equal to 5% and 15% of the total weight of the building, respectively. Thus, for a fair comparison, when CKBB control is used, the magnitude of the actuator force will be associated with the LDBI and HDBI as follows: for LDBI designs, $u_{max} = F_y = 14.46$ kN, and for HDBI designs, $u_{max} = F_y = 43.39$ kN. Furthermore, in this study, ideal actuator performance is assumed (i.e., the actuator can switch the direction of required forces at high speed, without time delay or actuator dynamics).

3.3 Ground Excitation

All of the accelerograms used in this study were scaled from accelerograms obtained from the Pacific Earthquake Engineering Research (PEER) Center Strong Motion Database [15]. Johnson et al. [23] and Spencer et al. [44] have recently raised concerns regarding the effectiveness of base isolation to protect structures against near-source, high-velocity, severe earthquakes. Hence, the library of earthquake records used in this study are partitioned into two classifications, moderate and severe earthquakes.

Moderate Ground Motion Accelerograms.

- 1940 El Centro – North-South component of the May 19, 1940, Imperial Valley, CA. USA. earthquake (unscaled magnitude 7.0). Recorded at the 117 El Centro Array #9 substation (United States Geological Survey (USGS) station 117). The closest distance of the substation to the fault rupture is 8.3 kilometers.

- 1979 El Centro – 3° North-North-West component of the October 15, 1979, Imperial Valley, CA. USA. earthquake (unscaled magnitude 6.5). Recorded at the 6618 Agrarias substation (Universi-

dad Nacional Autonoma de Mexico (UNAM)/ University of California San Diego (UCSD) station 6618). The closest distance of the substation to the fault rupture is 12.9 kilometers.

- 1987 Whittier – 9° North-North-West component of the October 1, 1987, Whittier, CA. USA. earthquake (unscaled magnitude 6.0). Recorded at the Arcadia - Campus Drive substation (University of Southern California (USC) station 90093). The closest distance of the substation to the fault rupture is 12.2 kilometers.

- 1992 Landers – East-West component of the June 28, 1992, Landers, CA. USA. earthquake (unscaled magnitude 7.3). Recorded at the 22170 Joshua Tree substation (California Division of Mines and Geology (CDMG) station 22170). The closest distance of the substation to the fault rupture is 11.6 kilometers.

The average distance to fault rupture is 11.2 kilometers.

Severe Ground Motion Accelerogram

- 1971 San Fernando – 164° South-South-West component of the February 9, 1971, San Fernando, CA. USA. earthquake (unscaled magnitude 6.6). Recorded at the 279 Pacoima Dam substation (CDMG station #279). The closest distance of the substation to the fault rupture is 2.8 kilometers.

- 1994 Northridge – East-West component of the January 17, 1994, Northridge, CA. USA. earthquake (unscaled magnitude 6.7). Recorded at the 24436 Tarzana, Cedar Hill substation (CDMG station 24436). The closest distance of the substation to the fault rupture is 17.5 kilometers.

- 1995 Kobe – North-South component of the January 16, 1995, Kobe, Japan earthquake (unscaled magnitude 6.9). Recorded at the Kobe Japanese Meteorological Agency (KJMA). The closest distance of the substatation to the fault rupture is 0.6 kilometers.

- 1999 Duzce – North-South component of the November 12, 1999, Duzce, Turkey earthquake (unscaled magnitude 7.1). Recorded at the 375 Lamont Doherty Earth Observatory substation. The closest distance of the substation to the fault rupture is 8.2 kilometers.

The average distance to fault rupture is 7.3 kilometers.

Ground Motion Scaling Procedure. Using peak ground acceleration (PGA) and Arias Intensity [4] as metrics of ground shaking severity (Arias Intensity is a measure of energy in the accelerogram), the

18

Earthquake	Scale Factor	Arias Intensity	Time at 90% AI (secs)	PGA (g)	Velocity (cm/sec) Min.	Velocity (cm/sec) Max.	Fourier Peak (secs)
1940 El Centro	1.031	1.43	10.52	0.323	-17.94	35.64	0.68
1979 El Centro	0.983	1.43	8.78	0.364	-33.60	24.08	0.53
1987 Whittier	1.296	1.43	2.54	0.388	-16.70	28.85	0.29
1992 Landers	1.140	1.43	12.78	0.324	-39.34	26.44	0.75
1971 San Fernando	1.186	12.07	6.62	1.451	-30.69	181.30	0.21
1994 Northridge	0.779	12.07	7.56	1.388	-104.30	44.08	0.35
1995 Kobe	1.205	12.07	6.04	0.989	-100.30	90.27	0.68
1999 Duzce	1.131	12.07	12.78	1.073	-44.34	32.76	0.34

Table 3.4: Scaled Components of Ground Motion Excitations

accelerograms were scaled so that they have approximately the same potential for imparting damage to a structure under moderate and severe ground motion events. The scaling procedure constrains each ground motion to have equal Arias Intensity and adjusts the scaling factors so that the average peak ground acceleration has a desired level. Mathematically, if $\ddot{x}_{ig}(t)$ is the i-th ground motion acceleration, then we seek scaling coefficients k_i so that:

$$\frac{\pi}{2g} \int_0^{15} k_1^2 \ddot{x}_{1g}^2(\tau) d\tau = \frac{\pi}{2g} \int_0^{15} k_2^2 \ddot{x}_{2g}^2(\tau) d\tau = \cdots = \frac{\pi}{2g} \int_0^{15} k_6^2 \ddot{x}_{6g}^2(\tau) d\tau = \text{constant}. \quad (3.1)$$

The scaled design ground motions were obtained by first isolating the worst fifteen-second sample of each record. Each record was then translated along the y-axis to remove residual velocity effects. Moderate and severe earthquake records were then scaled in the following manner:

1. **Moderate Earthquake Events.** The first group of earthquake records were scaled to an average peak ground acceleration (PGA) of 0.35g. The resultant Arias Intensity for these scaled earthquakes is 1.438 m/sec. The scaled accelerograms and corresponding Fourier Spectra are shown in Figures 3.4 and 3.6, respectively.

2. **Severe Earthquake Events.** The second group of earthquake records were scaled to an average PGA of 1.225g. The resultant Arias Intensity for these scaled earthquakes was 12.07 m/sec. The scaled accelerograms and Fourier Spectra are shown in Figures 3.5 and 3.7, respectively.

Time histories of Arias Intensity (m/sec) versus time (sec) for the moderate and severe ground motions are shown in Figures 3.8 and 3.9, respectively.

Table 3.4 shows results of the scaling procedures, including the ground motion scaling factor, Arias Intensity, time at which 90% of AI is achieved, PGA, minimum and maximum ground velocities,

and the period at which the peak Fourier transform occurs. Average PGA's of 0.35g and 1.225g for moderate and severe earthquake events is based on the recommendations of Park and Otsuka [34] and Ramallo et al. [38]. The Fourier transform is a frequency domain analysis technique that is used to determine dominant frequency.
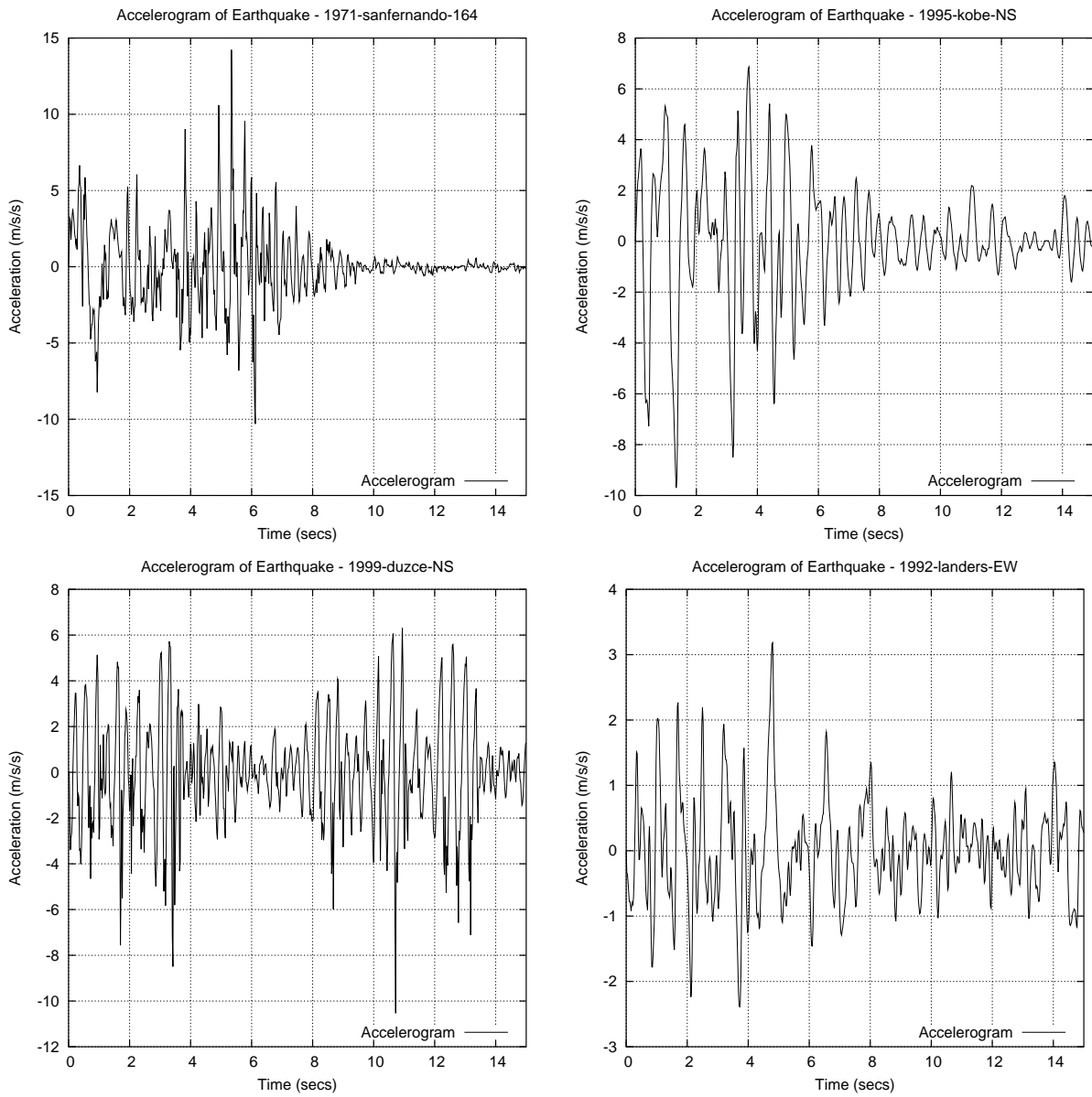
Figure 3.4: Moderate Ground Motion Accelerograms: (1) 1940 El Centro, (2) 1979 El Centro, (3) 1987 Whittier, and (4) 1992 Landers
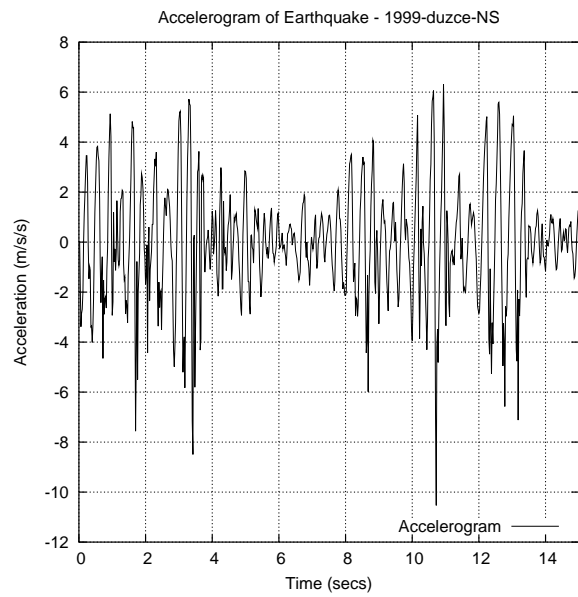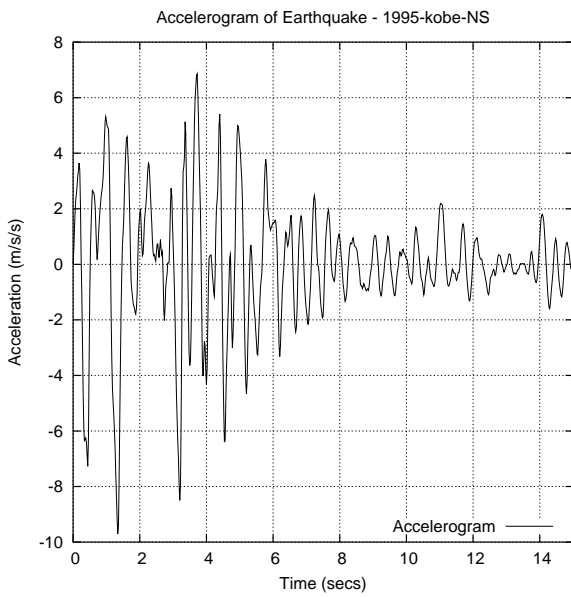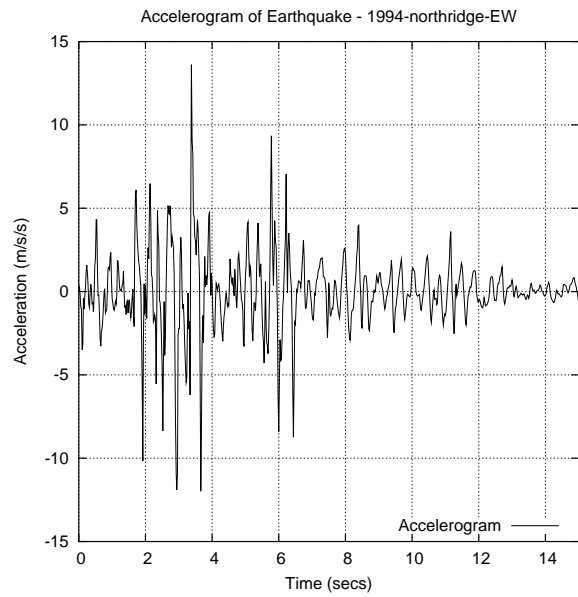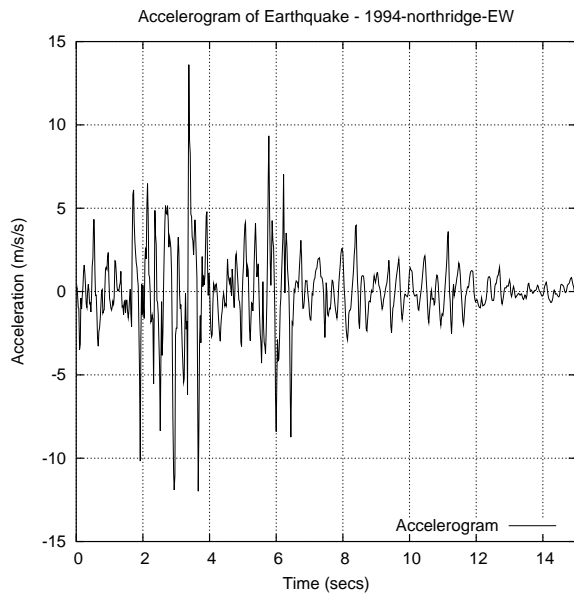
Figure 3.5: Severe Ground Motion Accelerograms: (1) 1971 San Fernando, (2) 1994 Northridge, (3) 1995 Kobe, and (4) 1999 Duzce
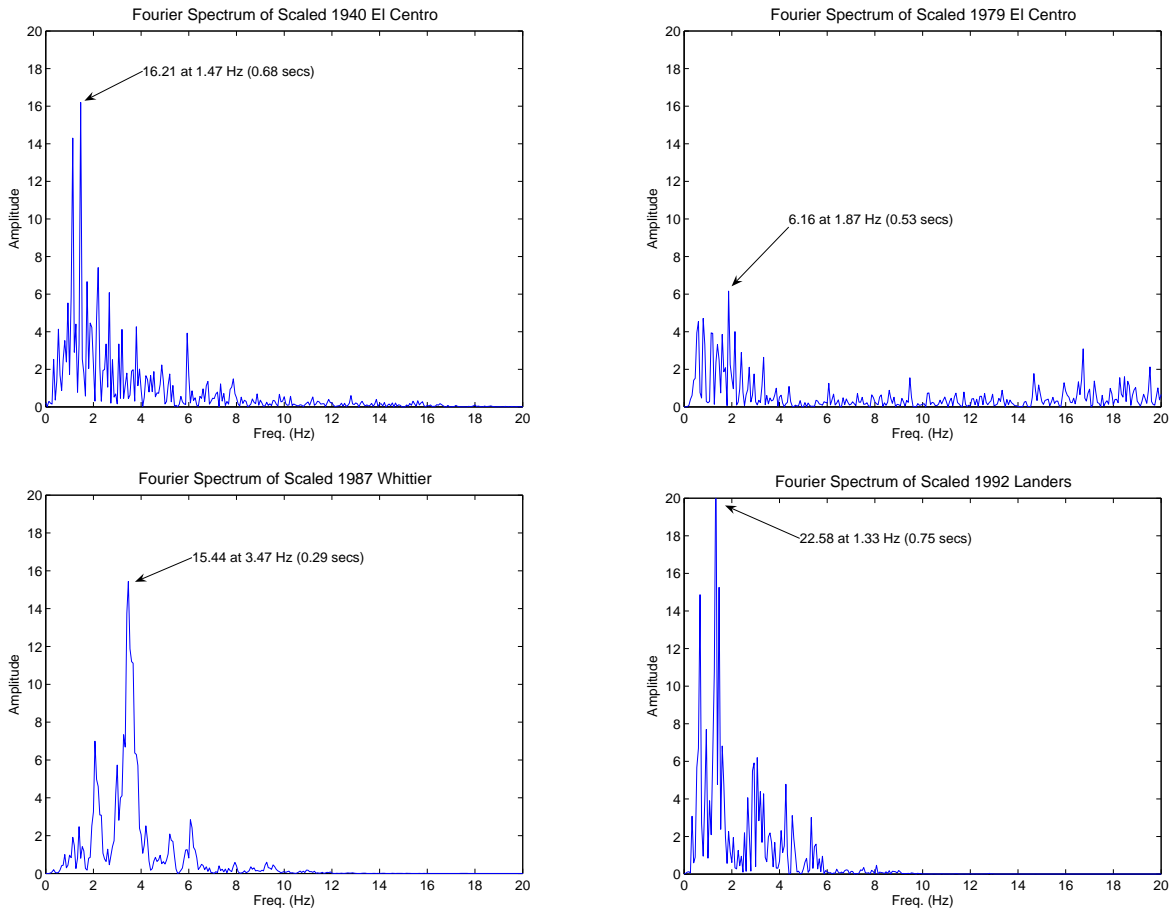
Figure 3.6: Fourier Spectra vs Frequency (Hz) for Moderate Ground Accelerograms. (1) 1940 El Centro, (2) 1979 El Centro, (3) 1987 Whittier, and (4) 1992 Landers.
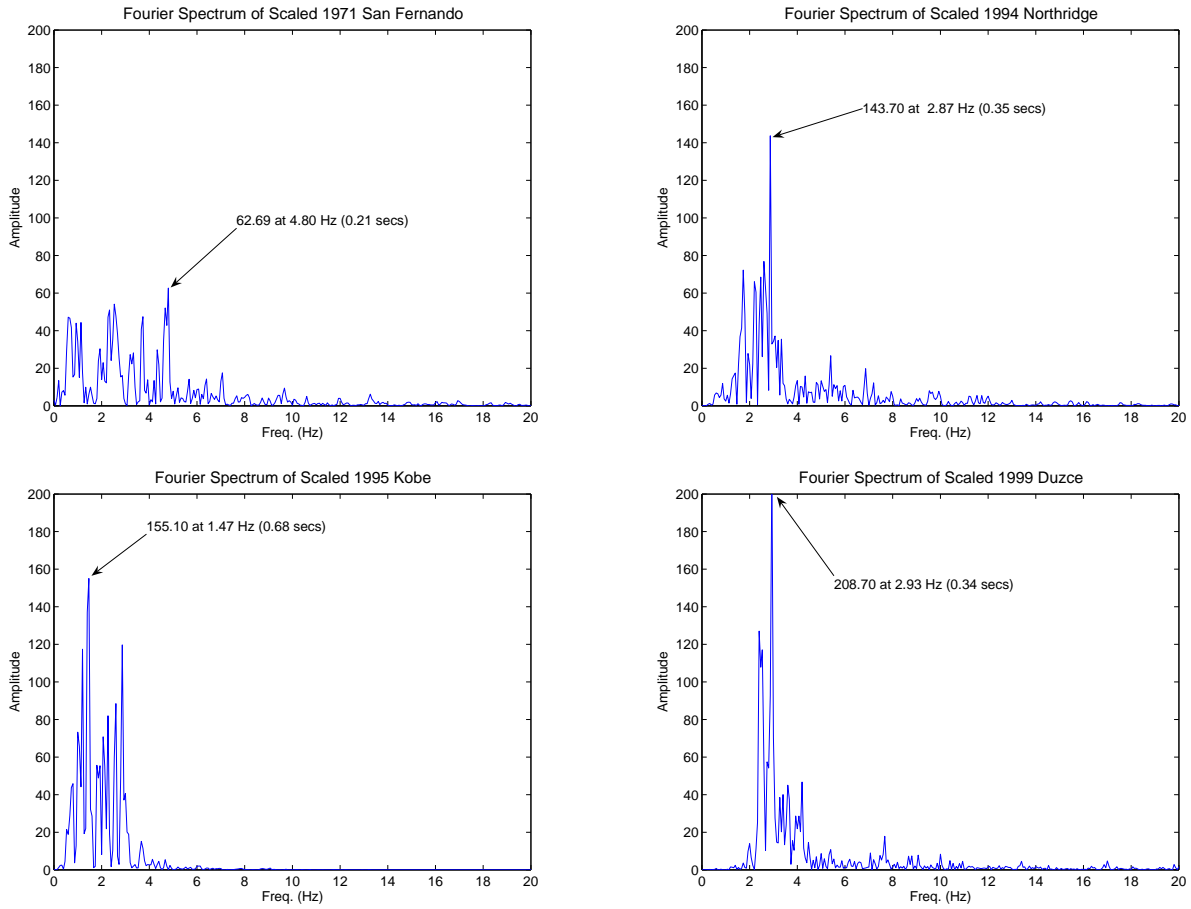
Figure 3.7: Fourier Spectra vs Frequency (Hz) for Severe Ground Accelerograms. (1) 1971 San Fernando, (2) 1994 Northridge, (3) 1995 Kobe, and (4) 1999 Duzce.
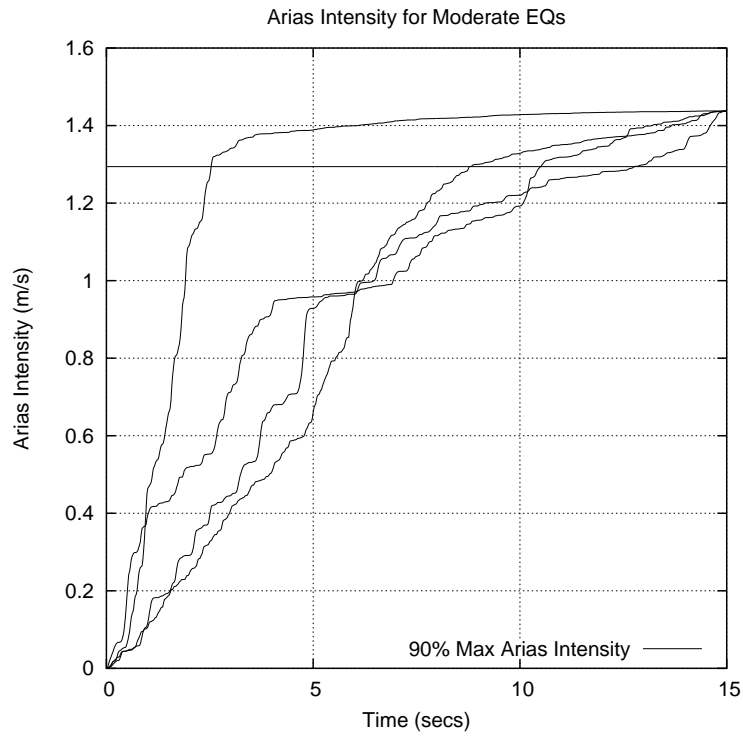
Figure 3.8: Arias Intensity (m/s) versus time (sec) for Moderate Ground Motions.
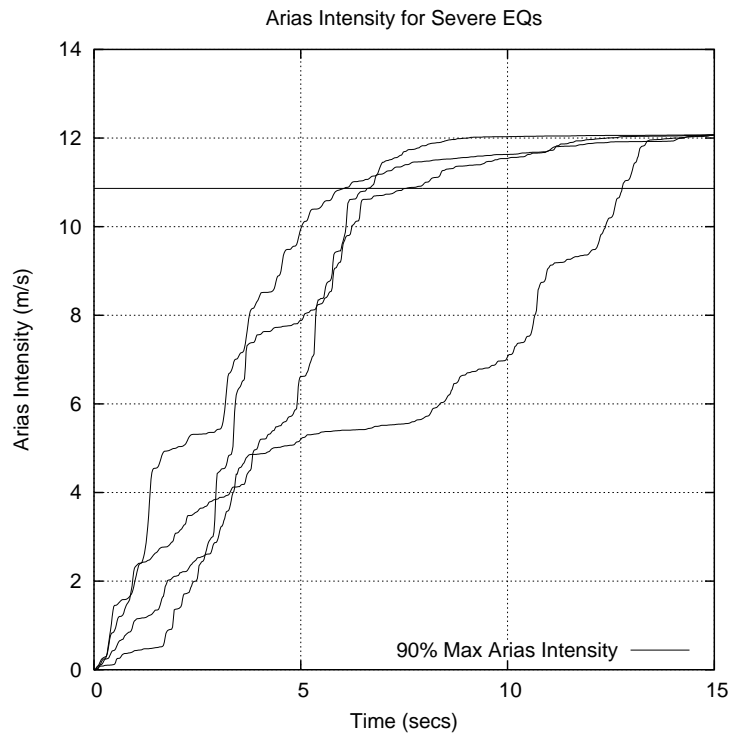
Figure 3.9: Arias Intensity (m/s) versus time (sec) for Severe Ground Motions.

25

3.4 Results of Numerical Experiment

The objectives of the numerical experiments are two-fold: (1) To identify situations when CKBB control is most likely to "add value" to system responses due to base isolation alone, and (2) To quantitatively determine the work done and power required by the actuator. Assessment of these factors is complicated by variations in design methodology for proportioning structural elements in seismic design, and significant uncertainties in predicting the size and nature of future ground motion events. Accordingly, the simulation results for our scaled 6-DOF model are organized into four practical scenarios:

1. A moderate severity BI/CKBB control design (LDBI and LDBI+CKBB) subjected to a moderate ground excitation (a El Centro characteristic earthquake),

2. A moderate severity BI/CKBB control design (LDBI and LDBI+CKBB) subjected to a severe ground excitation,

3. A high severity BI/CKBB control design (HDBI and HDBI+CKBB) subjected to a moderate ground excitation, and

4. A high severity BI/CKBB design (HDBI and HDBI+CKBB) subjected to a a severe ground excitation (a Northridge characteristic earthquake).

Design cases 1 and 4 cover the scenarios of expected ground motion attack. Design cases 2 and 3 are the scenario counter-examples.

Tables 3.5 through 3.8 show the peak base drifts, isolator work done, structural drifts, structural work done, actuator work done, and actuator power requirements for sets of system responses in each of these scenarios. We expect that by itself, the base isolation system will protect the superstructure by concentrating lateral displacements within the isolator elements. We also expect that the actuator will work to reduce the overall impact of external forces on the base isolated system. This phenomenon is recorded through plots of work done by the actuator (kJ) versus time (sec). A negative slope indicates that the actuator works to extract energy from the external excitations – in other words, negative slopes mean that the actuator is working like a damping mechanism. A positive slope corresponds to energy input. We know from our preliminary studies that if the actuator is not turned off after the main segments of ground shaking are over, then the actuator will feed energy into the system and in many cases, actually make the system response worse. To circumvent this problem, we terminate the actuator when the Arias Intensity for each scaled ground motion input reaches 90% of its final value.

26

Earthquake	Base Drift (mm)		Structural Drift (mm)		Isolator Work (kJ)		Structural Work (kJ)		Actuator Work (kJ)	Actuator Power (kW)
	LDBI	LDBI+ CKBB	LDBI	LDBI+ CKBB	LDBI	LDBI+ CKBB	LDBI	LDBI+ CKBB	LDBI+ CKBB	LDBI+ CKBB
1940 El Centro	79.8	45.89	0.77	1.88	10.44	6.91	2.33	2.42	-8.46	5.68
1979 El Centro	155.8	68.03	1.22	1.74	14.28	4.34	4.43	2.37	-4.19	5.45
1987 Whittier	72.6	33.50	0.74	1.64	2.35	1.48	1.32	2.12	-2.90	4.70
1992 Landers	162.3	125.90	1.25	1.77	20.21	11.14	6.05	3.49	-12.78	6.67
Average value:	117.6	68.33	0.99	1.75	11.82	5.96	3.53	2.60	-7.08	5.62

Table 3.5: Design Case 1. Peak Values of system response for LDBI and LDBI+CKBB subjected to Moderate Ground Motions

27

Earthquake	Base Drift (mm)		Structural Drift (mm)		Isolator Work (kJ)		Structural Work (kJ)		Actuator Work (kJ)	Actuator Power (kW)
	LDBI	LDBI+ CKBB	LDBI	LDBI+ CKBB	LDBI	LDBI+ CKBB	LDBI	LDBI+ CKBB	LDBI+ CKBB	LDBI+ CKBB
1971 San Fernando	529.8	454.50	3.26	3.26	59.27	45.77	52.08	41.48	-37.96	24.27
1994 Northridge	238.8	211.00	1.79	1.92	21.17	17.81	12.27	12.13	-18.88	12.87
1995 Kobe	354.6	251.50	2.36	2.19	49.69	42.33	38.93	26.93	-33.86	18.65
1999 Duzce	39.2	43.02	0.80	2.41	5.16	4.44	3.01	4.97	-14.47	6.40
Average value:	290.6	240.0	2.05	2.44	33.8	27.58	26.57	21.37	-26.3	15.54

Table 3.6: Design Case 2. Peak Values of system response for LDBI and LDBI+CKBB Subjected to Severe Ground Motions

3.4.1 Design Case 1. LDBI and LDBI+CKBB Control Subject to Moderate Ground Excitations

       This scenario corresponds to the system responses generated when LDBI and LDBI+CKBB designs are subject to moderate ground excitations. Ramallo et al. [38] found that LDBI was optimally designed to minimize base drift and structural acceleration for El Centro (moderate, i.e., PGA ~0.35g) characteristic ground excitations. Figures 3.12 through 3.16 show time histories of base drifts, base isolator hysteresis, base isolator work done, superstructure work done, actuator work done, and actuator power requirements. Table 3.5 summarizes the peak values of system response generated by four ground motions used in this scenario. In comparing the systems responses for LDBI+CKBB control and LDBI alone, it is evident that for all earthquakes, CKBB control reduces peak values of base drift. The average percentage of base drift reduction is 44%. Reductions in peak values of base drift are accompanied by marginal increases in the peak structural drift. In all cases, however, the magnitude of peak drifts in the isolator is much larger than in the superstructure (i.e., the isolator system is working the way it's supposed to!).

       CKBB control also affects the work done by the base isolator and superstructure. For all earthquake inputs, adding control decreases the work done by the base isolator. However, adding control decreases the work done by the superstructure in only half of the system responses. The average value of work done by the actuator is 7.08 kJ. The average value of power requirements is 5.63 kW.

3.4.2 Design Case 2. LDBI and LDBI+CKBB Control Subject to Severe Ground Excitations

       This scenario corresponds to system responses generated when LDBI and LDBI+CKBB designs are subject to unexpectedly severe, yet conceivable, ground motions (i.e., PGA ~1.225g). Figures 3.17 through 3.22 show time histories of base drift, base isolator hysteresis, base isolator work done, superstructure work done, actuator work done and actuator power requirements. Table 3.6 summarizes the peak values of system response generated by the four ground motions used in this scenario. With the exception of the 1999 Duzce case study, the peak values of base drift were reduced with the addition of CKBB control Peak base drifts are reduced, on average, by 11%. Peak values of structural drift were virtually unchanged, except for the 1999 Duzce which resulted in a tripling of peak structural drift. Notice, however, that peak values of structural drift under 1999 Duzce are no larger than for the other three ground motion inputs and, in fact, peak drifs in the isolator (although slightly larger) are considerably smaller than for the San Fernando, Northridge and Kobe inputs. We surmise that this anomaly might be

due to the extended duration of actuator action – the 90% AI for 1999 Duzce occurs at 12.78 seconds. The maximum duration of actuator application among the remaining three earthquakes is 7.56 seconds.

In all cases, the addition of control reduces the work done by the isolator element, and in 3 out of 4 cases, also work done by the superstructure. Measured across the four ground motion inputs, the average work done and power required by the actuator are 26.29 kJ and 15.55 kW, respectively.

3.4.3 Design Case 3. HDBI and HDBI+CKBB Control Subject to Moderate Ground Excitations

The United States Geological Survey (USGS) tracks numerous earthquakes everyday from around the world of magnitude>5.0 at its website [53]. Small and moderate sized earthquakes occur much more frequently than severe earthquakes, This scenario occurs when HDBI and HDBI+CKBB designs are attacked by moderate ground excitations (i.e., a base isolated structure is designed for a severe ground motion, but is subjected to a more likely moderate earthquake.)

Figures 3.23 through 3.28 shows time histories of base drift, base isolator hysteresis, base isolator work done, superstructure work done, actuator work done, and actuator power requirements. Table 3.6 summarizes the peak values of system response quantities generated by the four ground motion inputs.

With the exception of the 1971 San Fernando time-history response, system responses for this case study are almost elastic. The isolator yield displacement is 43.39 kN/2,320 kN/m = 18.7 mm. Three of the four records have a displacement ductility of less than 1.65. The exception is the 1971 San Fernando time-history response, which generates a displacement ductility of 2.87. In all cases, peak values of base drift are reduced – the average reduction is 52% – through the addition of CKBB control As with the other design cases, reductions in base drift are accompanied by increases in structural drift. The addition of CKBB control decreases the amount of work done by the base isolator, but increases work done by the superstructure – on average, work done by the superstructure increases by 349%. The average value of work done by the actuator is 5.85 kJ. The average value of power requirements is 11.54 kW.

3.4.4 Design Case 4. HDBI and HDBI+CKBB Control Subject to Severe Ground Excitations

This scenario occurs when HDBI and HDBI+CKBB designs are attacked by severe ground excitations. Park and Otsuka [38] found that HRBI was optimally designed to for Northridge characteristic

	Base Drift (mm)		Structural Drift (mm)		Isolator Work (kJ)		Structural Work (kJ)		Actuator Work (kJ)	Actuator Power (kW)
Earthquake	HDBI	HDBI+CKBB	HDBI	HDBI+CKBB	HDBI	HDBI+CKBB	HDBI	HDBI+CKBB	HDBI+CKBB	HDBI+CKBB
1940 El Centro	71.1	30.83	1.74	5.16	22.06	1.46	4.07	14.03	5.43	9.37
1979 El Centro	74.6	23.17	1.57	4.40	11.35	0.86	1.70	12.69	8.36	7.43
1987 Whittier	56.3	28.16	1.74	4.86	6.96	3.49	4.02	4.02	-4.51	18.77
1992 Landers	79.2	53.72	1.67	4.39	24.77	3.10	2.89	17.49	5.09	10.58
Average value:	70.3	33.9	1.68	4.70	16.3	2.59	5.61	12.05	3.59	11.5

Table 3.7: Design Case 3. Peak Values of system response for HDBI and HDBI+CKBB subjected to Moderate Ground Excitation

30

	Base Drift (mm)		Structural Drift (mm)		Isolator Work (kJ)		Structural Work (kJ)		Actuator Work (kJ)	Actuator Power (kW)
Earthquake	HDBI	HDBI+CKBB	HDBI	HDBI+CKBB	HDBI	HDBI+CKBB	HDBI	HDBI+CKBB	HDBI+CKBB	HDBI+CKBB
1971 San Fernando	424.5	276.00	3.59	4.68	97.23	45.62	38.23	17.77	-62.10	47.54
1994 Northridge	173.0	105.90	2.21	4.26	34.27	23.03	13.78	12.15	-42.90	38.68
1995 Kobe	188.2	220.70	2.80	4.36	104.40	72.28	23.77	20.90	-73.99	52.82
1999 Duzce	68.6	42.53	1.97	5.00	7.10	4.20	5.83	14.20	-36.31	20.63
Average value:	213.6	161.3	2.64	4.57	60.7	36.3	20.4	16.3	-53.8	39.9

Table 3.8: Design Case 4. Peak Values of system response for HDBI and HDBI+CKBB subjected to Severe Ground Excitation

ground excitations. This HRBI design is not common in practice, but due to the significant concern (see, for example, comments by Hall et al. [18], Heaton et al. [19], and Spencer et al. [44]) of base-isolated buildings to accommodate severe near-fault earthquakes this alternative design is considered in this study. Figures 3.29 through 3.34 show time histories of base drift, base isolator hysteresis, base isolator work done, superstructure work done, actuator work done, and actuator power requirements. Table 3.6 summarizes the peak values of system response generated by the four ground motions used in this scenario.

With the exception of the 1995 Kobe input, the peak base drift was reduced when HDBI+CKBB control versus HDBI alone was used; the average percentage of this base drift reduction was 24%. This reduction in peak base drift was associated with modest increases in the peak structural drift. For all earthquakes used, the peak amount of work done by the base isolator decreased, and in 3 out of 4 earthquakes, the work done by the superstructure decreased when HDBI+CKBB control was used. The average work done and power required by the actuator are 53.83 kJ and 39.92 kW, respectively.

3.4.5 Sensitivity of System Performance to Systematic Variations in Design Methodology and Ground Motion Intensity

For design purposes we are interested in quantifying improvements in base isolation system response due to active control, and in identifying elements of system response that are insensitive to systematic variations in ground motion intensity and design methodology. We note that even if control does not decrease the overall magnitude of a particular response values, it can still be useful if it simply works to hold a response quantity steady, thereby making the estimation of peak response quantities more reliable.

The first metric is captured by the two-column format of response parameters in Tables 3.5-3.8. The second metric can be assessed by comparing parameters in Tables 3.5 and 3.6 (for LDBI and LDBI+CKBB) and Tables 3.7 and 3.8 (for HDBI and HDBI+CKBB). The third metric is orthogonal to the second and can be assessed by comparing parameters in Tables 3.5 and 3.7 (for moderate earthquake loads) and Tables 3.6 and 3.8 (for severe earthquake loads). The key observations are as follows.

Variation in Ground Motion Intensity

For design cases 1 and 3, moderate earthquake records were scaled to an average peak ground acceleration (PGA) of 0.35g. The resultant Arias Intensity for these scaled earthquakes is 1.438 m/sec. For design cases 2 and 4, severe earthquake records were scaled to an average PGA of 1.225g. The

31

resultant Arias Intensity for these scaled earthquakes was 12.07 m/sec. Looked a second way, on average, peak accelerations for the severe intensity ground motions are 3.5 (i.e., 1.225/0.35 = 3.5) times those of the moderate intensity ground motions. The corresponding severe/moderate ratio of Arias Intensities is 12.07/1.438 = 8.39 (note: recall that Arias Intensity is proportional to the square of ground acceleration).

Low Damping Base Isolator (LDBI) Design. Tables 3.5 and 3.6 show that as we move from moderate to severe ground motion intensity, peak values of base isolator displacement increase 247% and 351% under LDBI and LDBI+CKBB, respectively. Corresponding increases in structural drifts are 207% and 139%. Work done by the actuator increases 367%.

High Damping Base Isolator (HDBI) Design. Tables 3.7 and 3.8 show that as we move from moderate to severe ground motion intensity, on average, peak values of base isolator displacement increase 303% and 475% under HDBI and HDBI+CKBB, respectively. Corresponding increases in structural drifts are 157% and -2.7%. Work done by the actuator increases 1500%. As we will soon see, these percentage increases are amplified by the ineffective role of actuation for design case 3, where the actuators should simply be turned off!

Among the four simulation scenarios, design case 4 places the greatest demand on the actuator performance. Coincidentally, the addition of CKBB control offers significant opportunities for improvements to system-level performance.

Variation in Design Methodology

As explained in Section 3.2.1, the HDBI design is stiffer and significantly stronger than the LDBI design counterpart. The low damping base isolation (LDBI) design has $F_y = 14.46$ kN (which is 5% of the building weight) and $K_{initial}/K_{yield} = 6$. The isolator yield displacement is 14.46 kN/1,392 kN/m = 10.4 mm. The high damping base isolator (HDBI) design has a yield force of $F_y = 43.39$ kN = 15% of the building weight and a stiffness ratio of $K_{initial}/K_{yield} = 10$. The isolator yield displacement is 43.39 kN/2,320 kN/m = 18.7 mm. Both designs have same post-yield stiffness, as to give a post-yield period of 2.5 seconds. The LDBI+CKBB and HDBI+CKBB designs assume that control will not add value to the overall system performance unless the passive and active damping components can work in concert. Accordingly, as a first cut in research investigation, magnitude of the actuator force is tied to the yield force of the base isolators: for LDBI designs, $u_{max} = F_y = 14.46$ kN, and for HDBI designs, $u_{max} = F_y = 43.39$ kN.

Moderate Ground Motion Attack. For system responses generated by moderate ground motion attack,
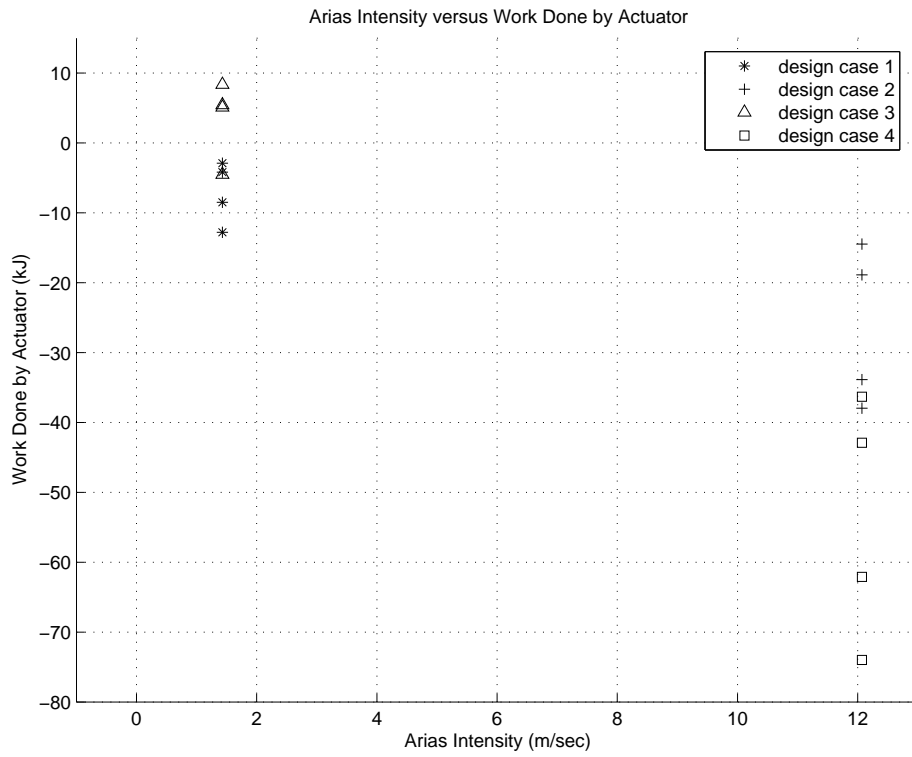
Figure 3.10: "Work done by actuator" (kJ) versus "Arias Intensity" (m/sec)
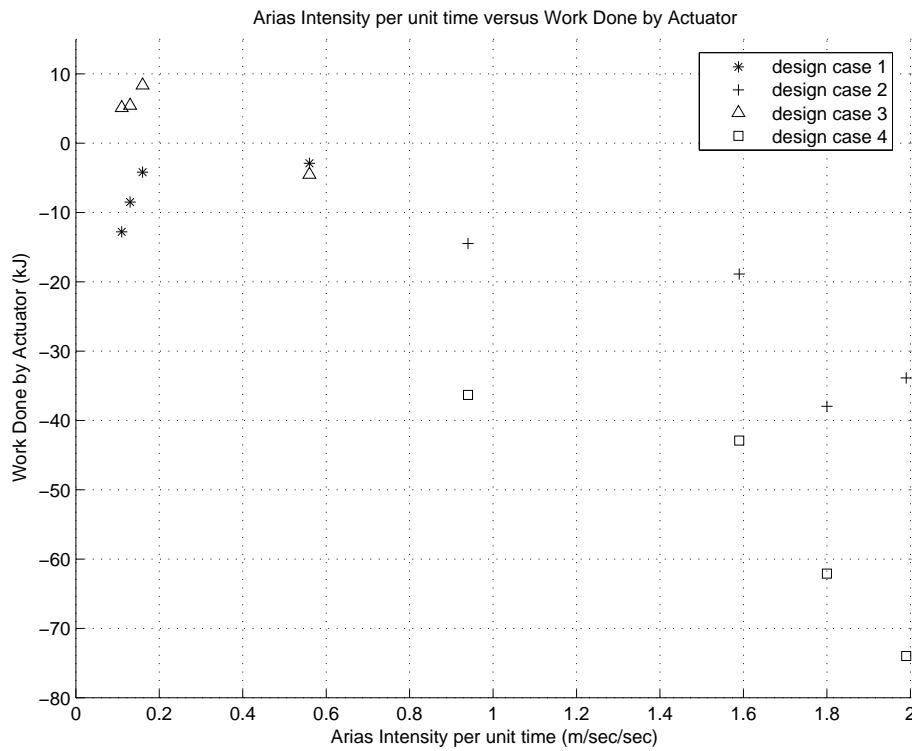
Figure 3.11: "Work done by actuator" (kJ) versus "Arias Intensity per unit time" (m/sec/sec)

aspects of system response (e.g., peak drifts, work done by the isolator, actuator work and power) are of the same order of magnitude in both designs. As required by the base isolation design, lateral drifts are concentrated in the isolator. Peak values of structural drift in the HDBI design (although still small) are almost twice those of the LDBI design – this phenonmenon can be simply attributed to the difference in base isolator yield forces and, hence, the ability of the HDBI design to transmit higher shear forces to the main structural system. In design cases 1 and 3, the magnitude of work done by the actuator is minor and, on the surface, inconsistent. In design case 1 (like design cases 2 and 4), the actuator works to extract small amounts on energy from the system input. Three of the four inputs have actuator work done that is positive, indicating that the actuator feeds input into the system. Drifts are nonetheless reduced by about 50%. Given that peak values of drift under HDBI design are less than half of those generated by LDBI+CKBB and HDBI+CKBB (i.e., design cases 2 and 4), under design scenario 3 the active control should simply be turned off!

As a first step toward understanding this phenomenon, Figure 3.10 shows "work done by the actuator" versus "Arias Intensity (m/sec)" for the system responses scaled to moderate and severe ground shaking intensity. Other than noting that "work done by the actuator" is smaller for design cases 2 and 1 than design cases 4 and 3, respectively, it is difficult to identify from Figure 3.10 cause-and-effect relationships that have practical meaning. Notice, however, that if we plot "work done by the actuator" versus "ground motion input energy (AI)/per unit time" the eight system responses for moderate ground shaking separate into two groups. See Figure 3.11. The smaller group of three responses corresponds to the three system responses where actuator input energy is positive. We already know from our previous work that the actuator will input energy into the system once the ground motion has stopped. This study suggests that input energy may also be positive for ground motions where "ground motion input energy (AI)/per unit time" is small.

Severe Ground Motion Attack. For system responses generated by severe ground motion attack, aspects of system response, peak values of structural drift under LDBI and HDBI alone are very similar. The addition of CKBB in design case 2 reduces peak values of base drift by 17% and work done by the isolator by 18%. Structural drifts increase by 16%. Even under the combination of passive and active control, maximum displacement ductilities cover the range [4.1, 43.5] and may be unacceptably high. For design case 4, reductions in "peak base drift" and "work done by the isolator" due to CKBB control are 24% and 40%, respectively. In all eight system responses (in design cases 2 and 4), work done by the actuator is negative.

On average, peak values of base drift for LDBI+CKBB (i.e., design case 2) are 149% larger than for design case 4. Corresponding values of work done by the actuator are -26.3 kJ and -53.8 kJ, respectively. The increase in work done by the actuator is partly due to the magnitude of applied actuator force (43.39 kN for HDBI+CKBB versus 14.46 kN for LDBI+CKBB) and, in part, to the increase in elastic stiffness of HDBI relative to LDBI.
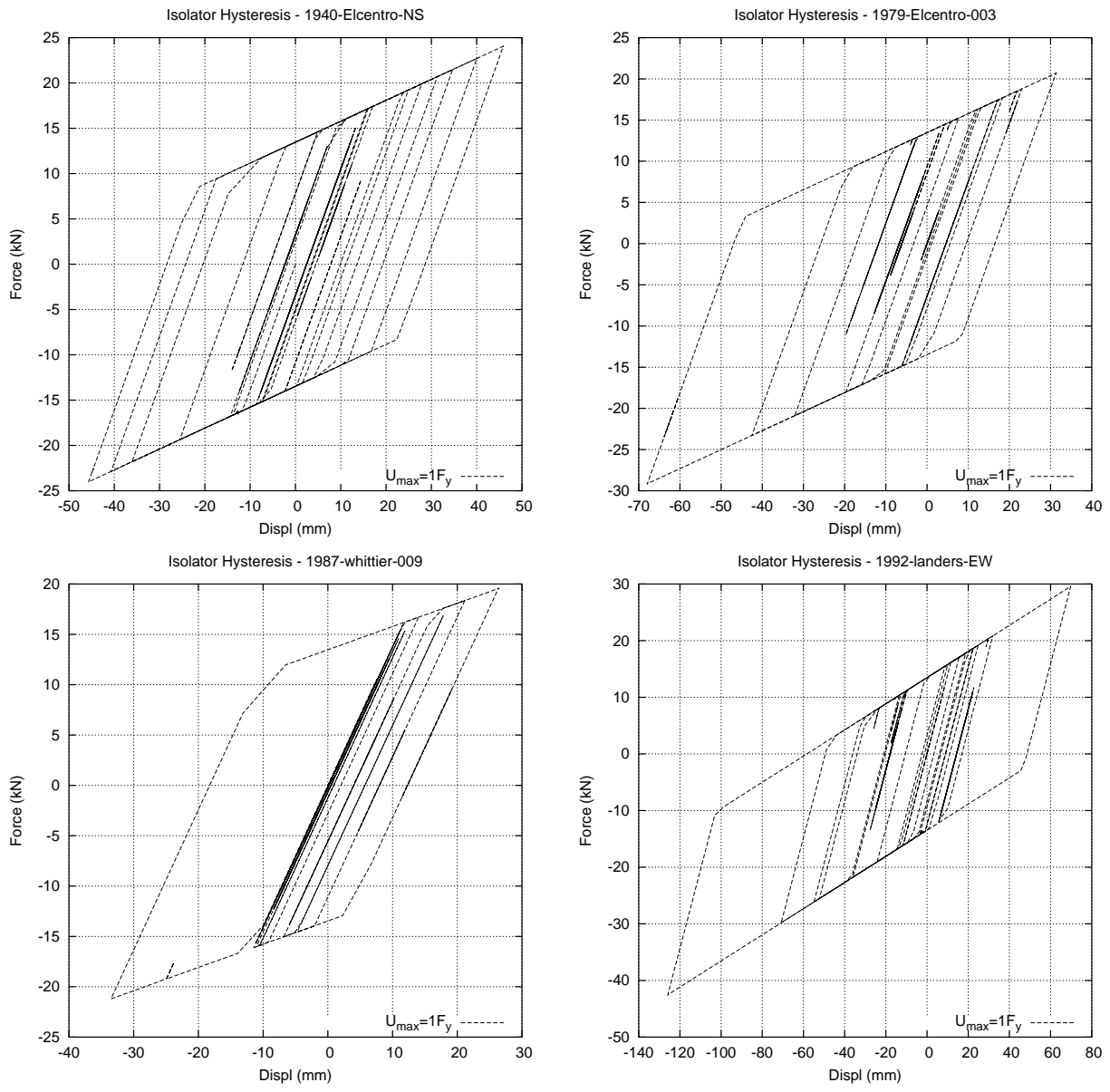
Figure 3.12: Design Case 1. LDBI+CKBB design subject to moderate ground excitations. Force-displacement hysteresis curves for LDBI+CKBB Design: 1940 El Centro, 1979 El Centro, 1987 Whittier, 1992 Landers.
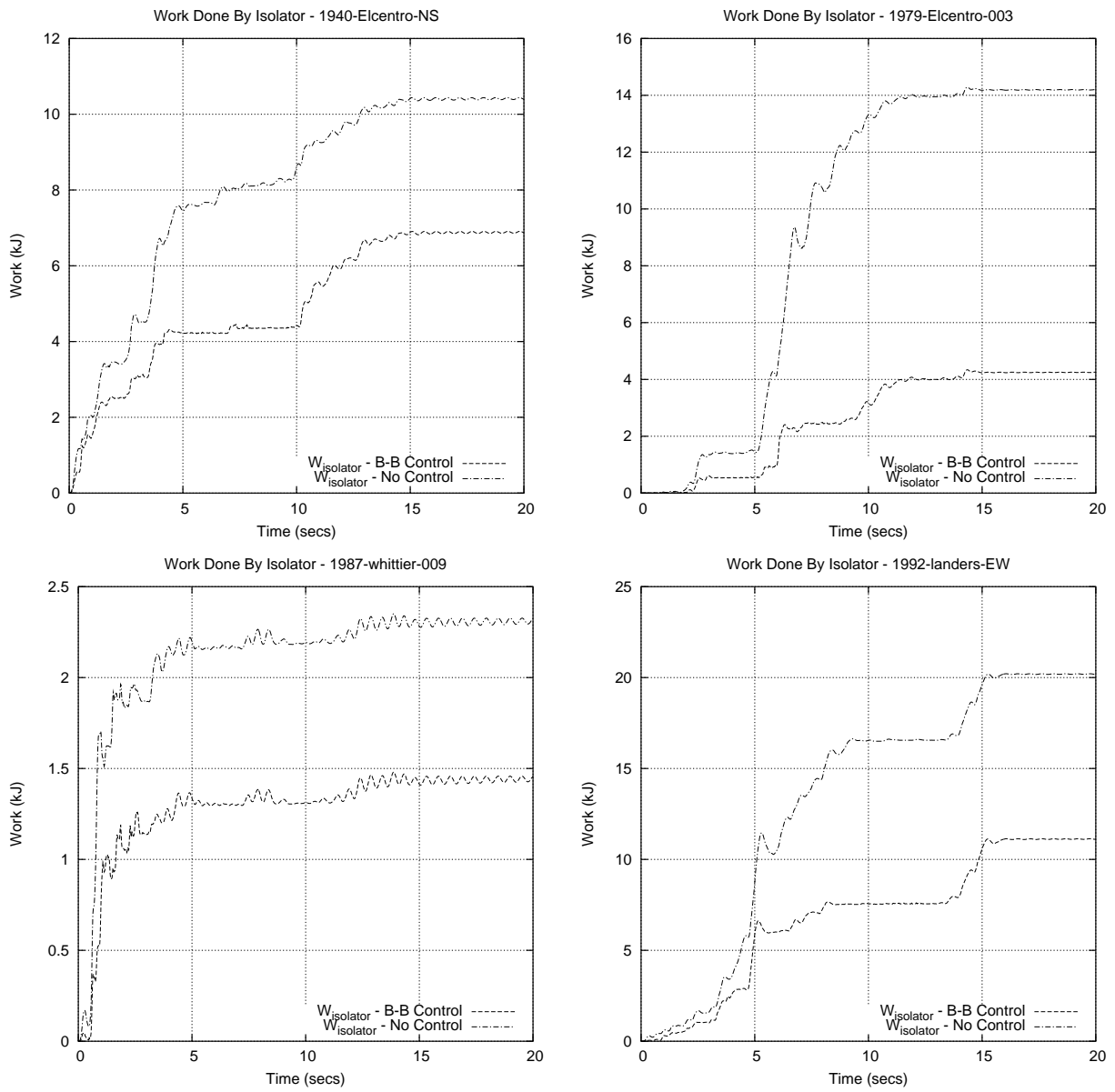
Figure 3.13: Design Case 1. LDBI and LDBI+CKBB designs subject to moderate ground excitations: 1940 El Centro, 1979 El Centro, 1987 Whittier, 1992 Landers. Comparison of base isolator work done (kJ) versus time (sec).
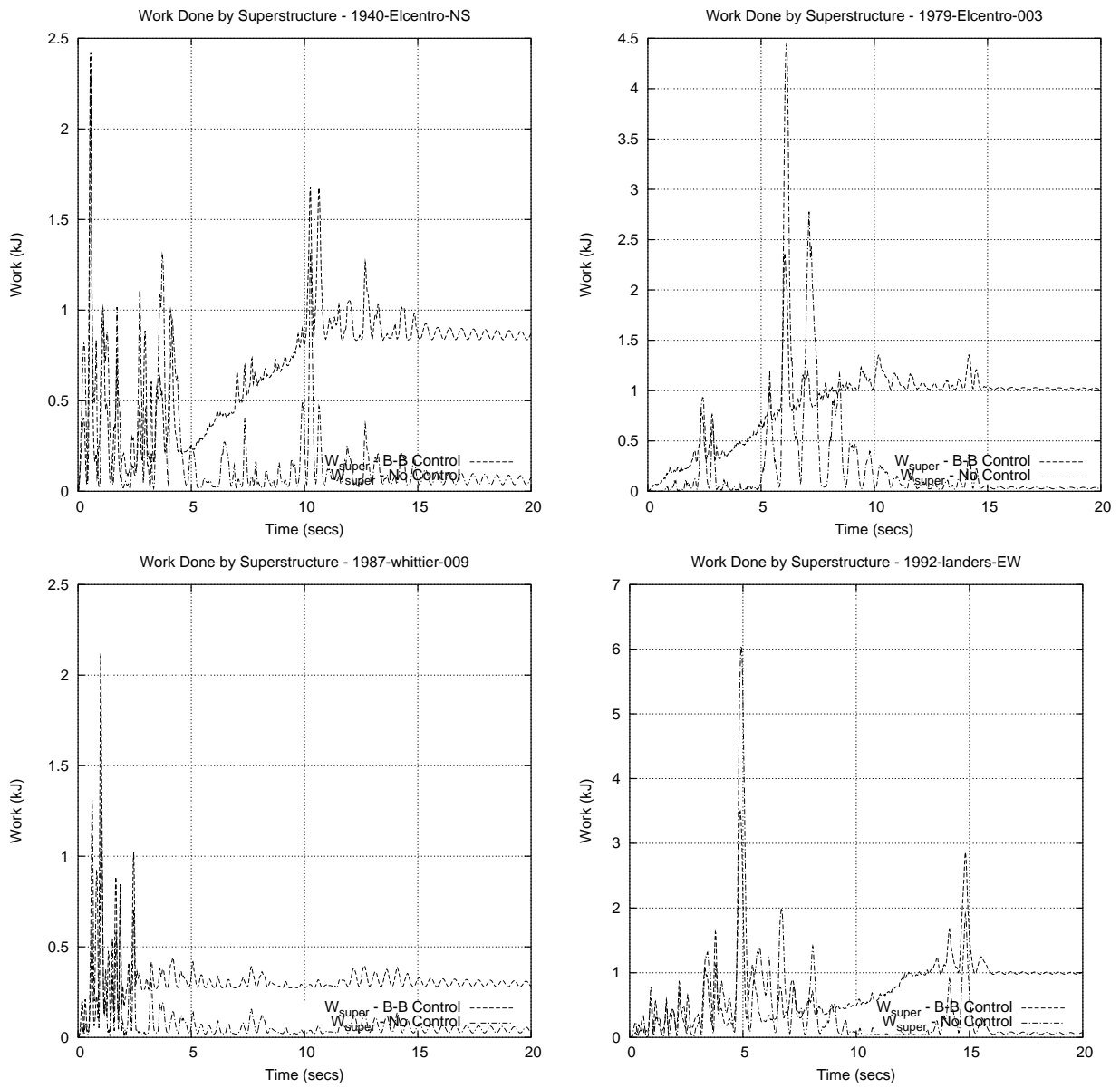
Figure 3.14: Design Case 1. LDBI and LDBI+CKBB designs subject to moderate ground excitations: 1940 El Centro, 1979 El Centro, 1987 Whittier, 1992 Landers. Comparison of superstructure work done (kJ) versus time (sec).
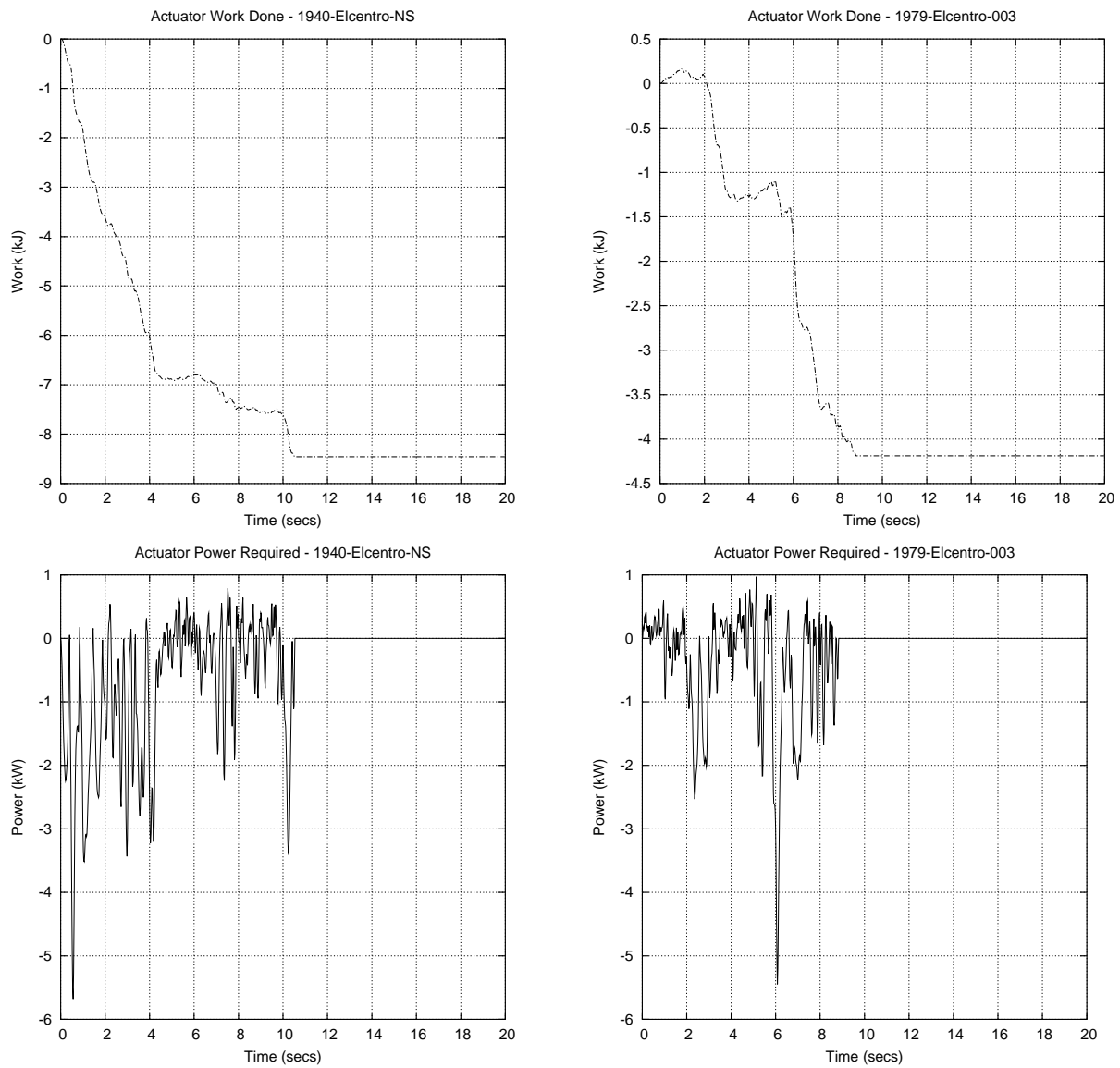
Figure 3.15: Design Case 1. LDBI+CKBB designs subject to moderate ground excitations: 1940 El Centro and 1979 El Centro. The upper graphs show actuator work done (kJ) versus time (sec). The lower graphs show power requirements (kW) versus time (sec).
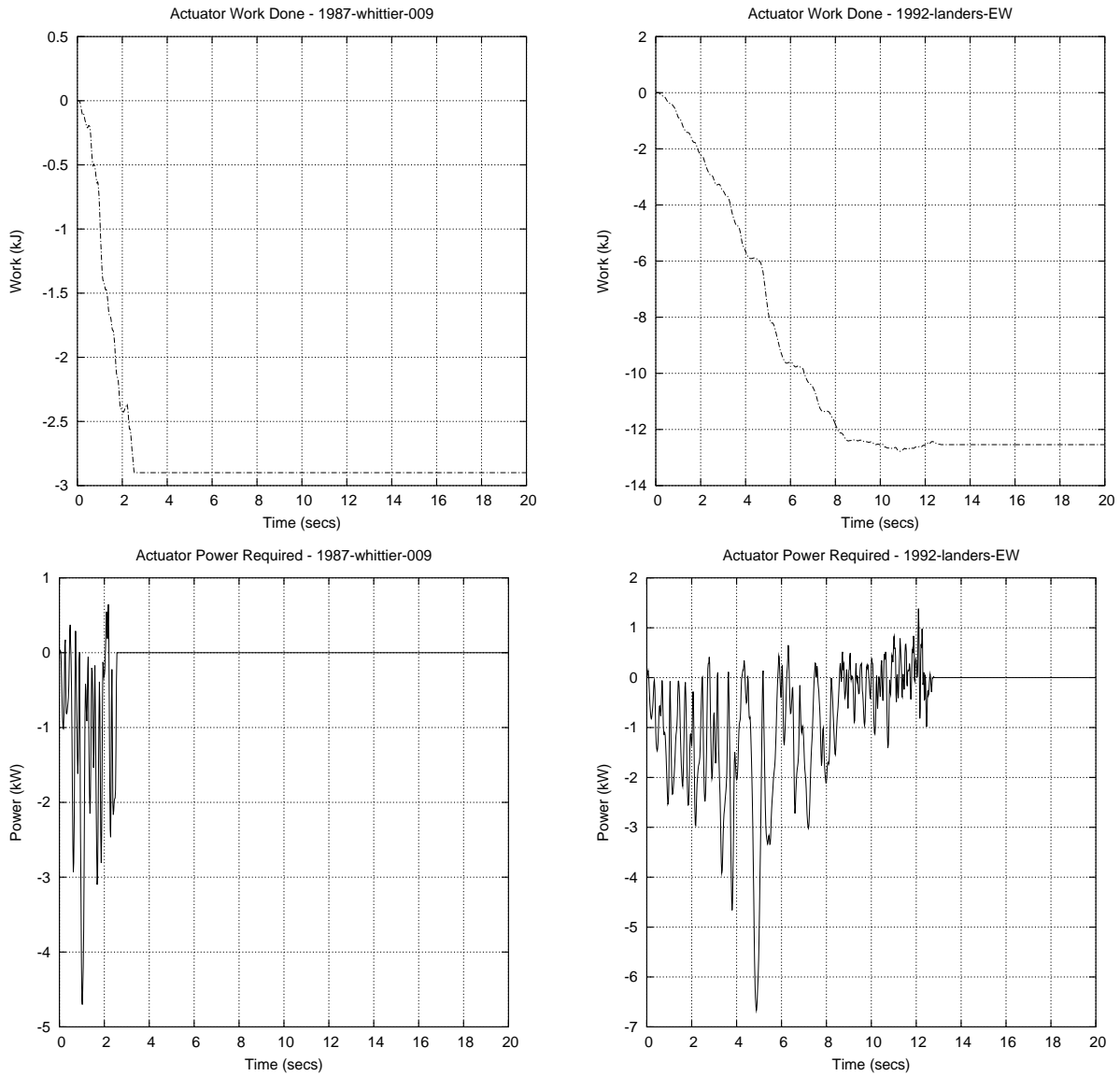
Figure 3.16: Design Case 1. LDBI+CKBB designs subject to moderate ground excitations: 1987 Whittier and 1992 Landers. The upper graphs show actuator work done (kJ) versus time (sec). The lower graphs show power requirements (kW) versus time (sec).

40
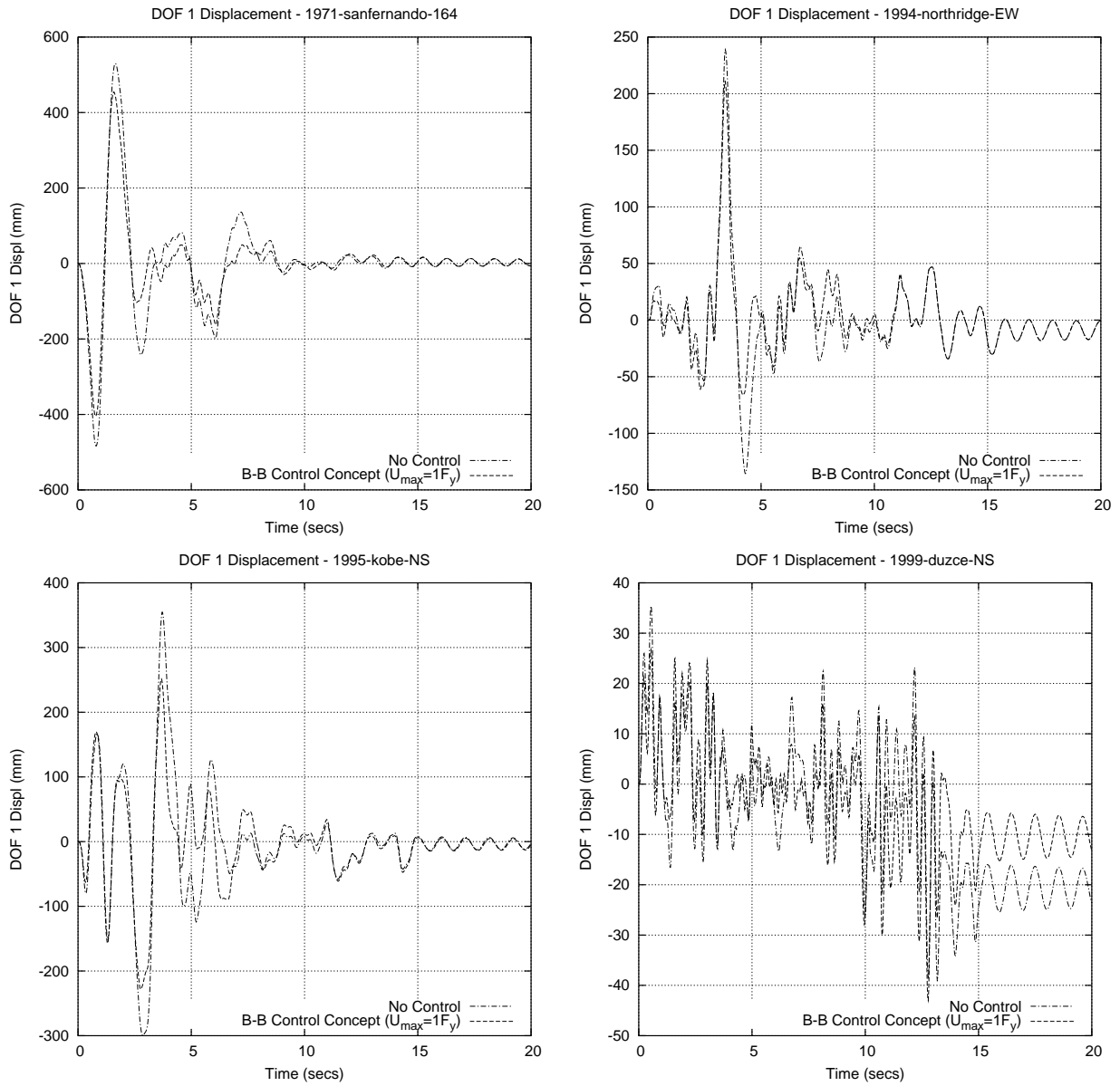
Figure 3.17: Design Case 2. LDBI and LDBI+CKBB designs subject to severe ground excitations: 1971 San Fernando, 1994 Northridge, 1995 Kobe, 1999 Duzce. Base isolator drift (mm) versus time (sec).
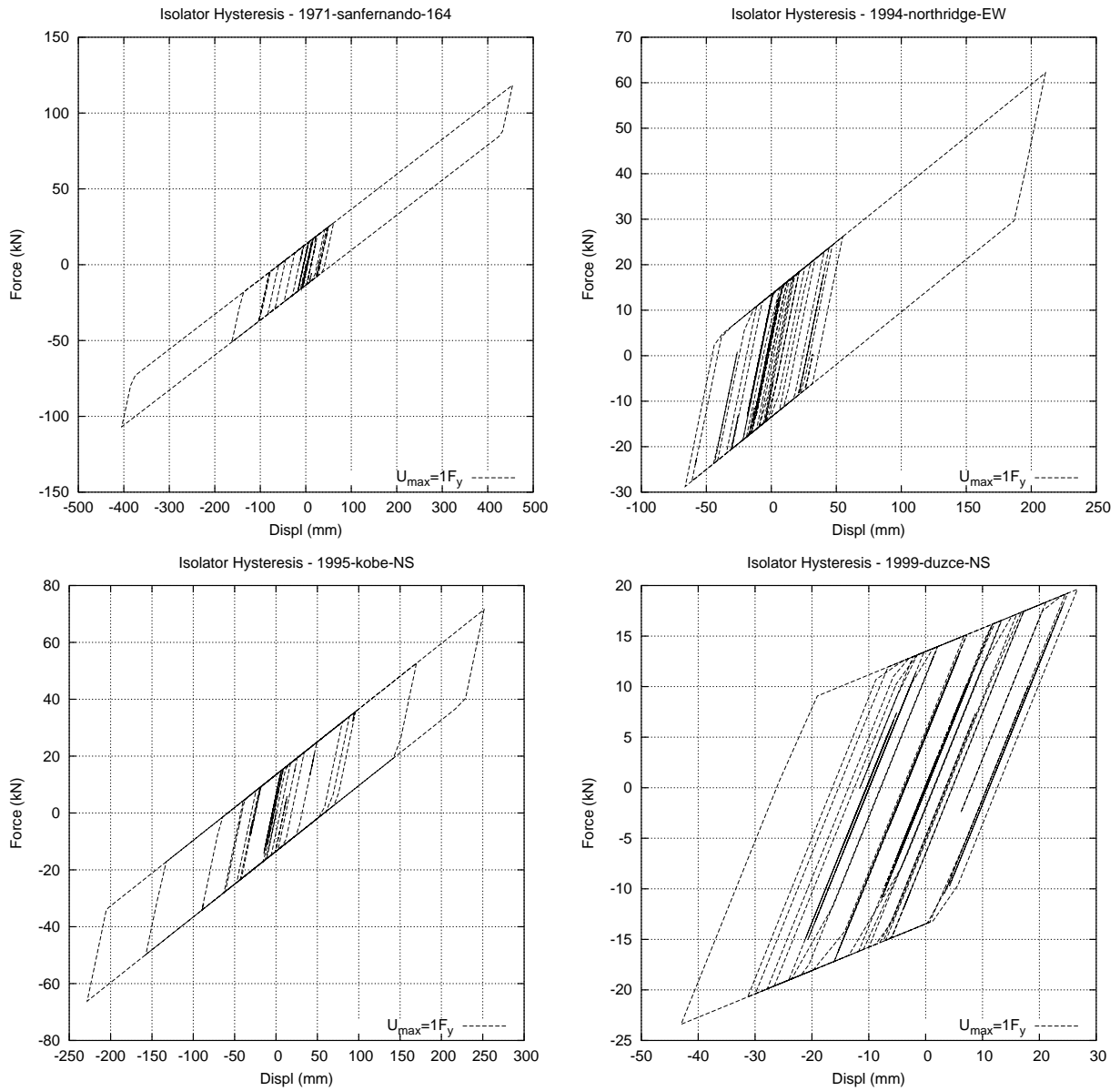
Figure 3.18: Design Case 2. LDBI and LDBI+CKBB designs subject to severe ground excitations: 1971 San Fernando, 1994 Northridge, 1995 Kobe, 1999 Duzce. Force-displacement hysteresis curves.
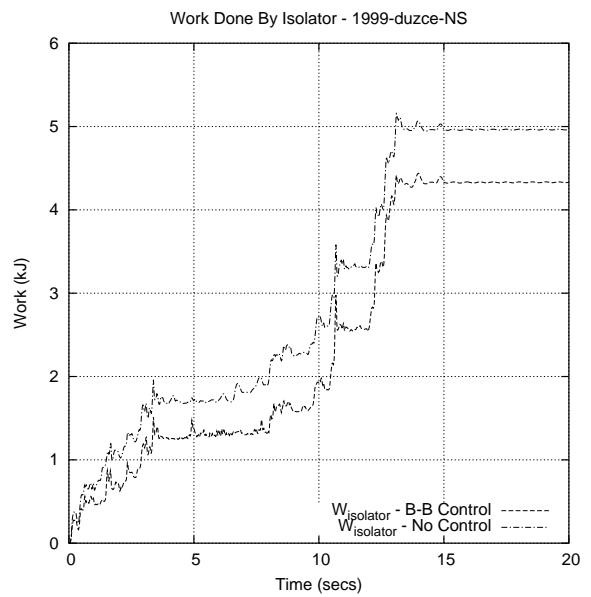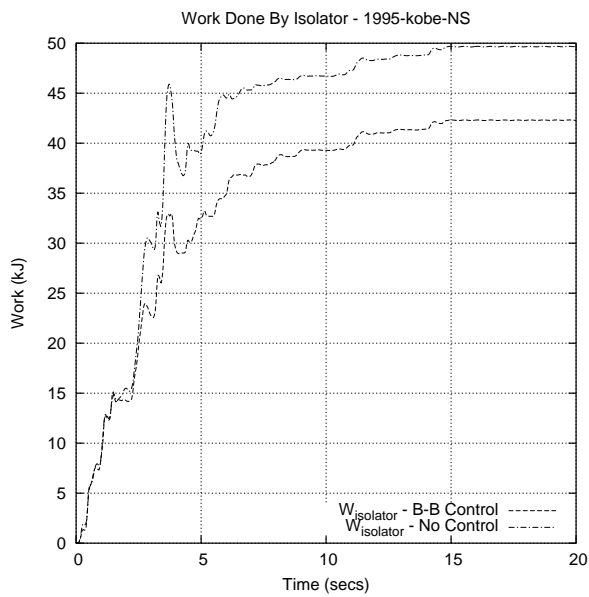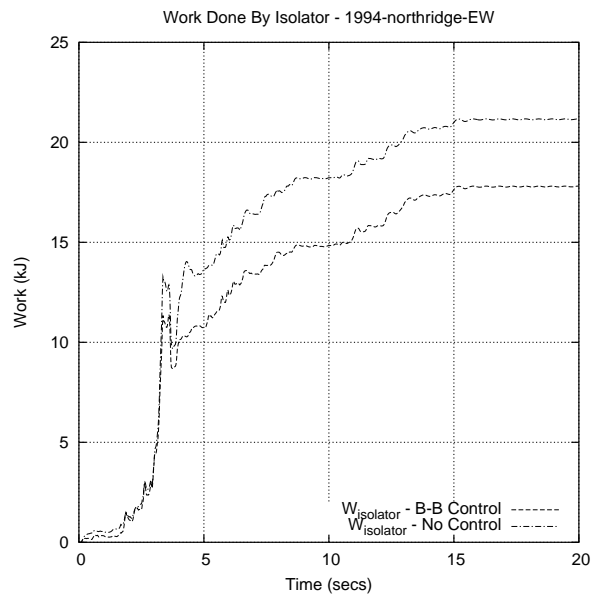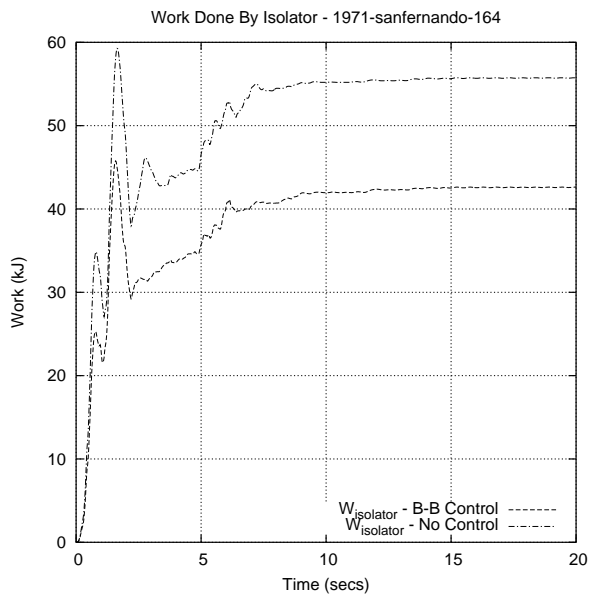
Figure 3.19: Design Case 2. LDBI and LDBI+CKBB Designs subject to severe ground excitations: 1971 San Fernando, 1994 Northridge, 1995 Kobe, 1999 Duzce. Base isolator work done (mm) versus time (sec).

43
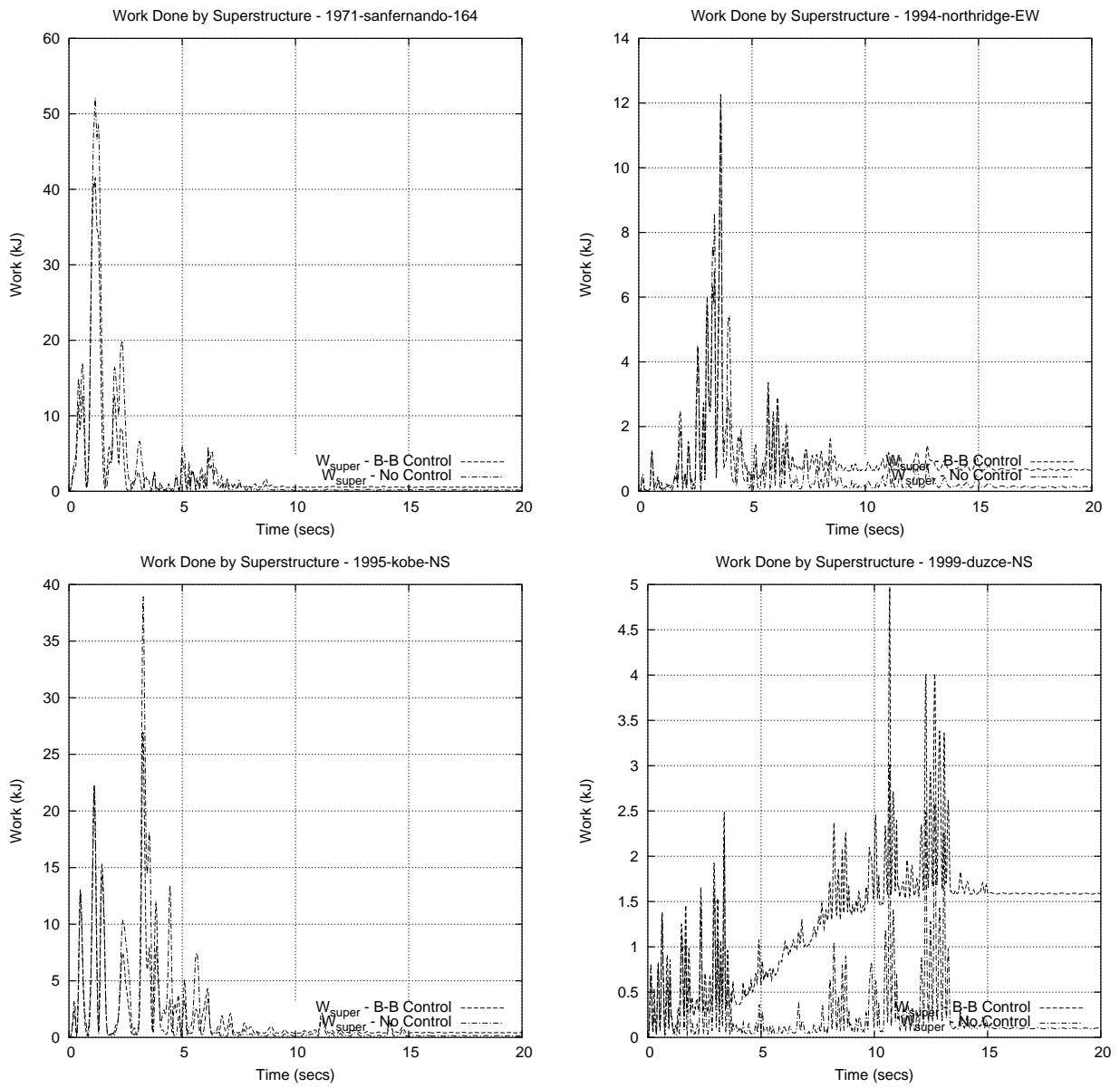
Figure 3.20: Design Case 2. LDBI and LDBI+CKBB Designs subject to severe ground excitations: 1971 San Fernando, 1994 Northridge, 1995 Kobe, 1999 Duzce. Superstructure work done (kJ) versus time (sec).
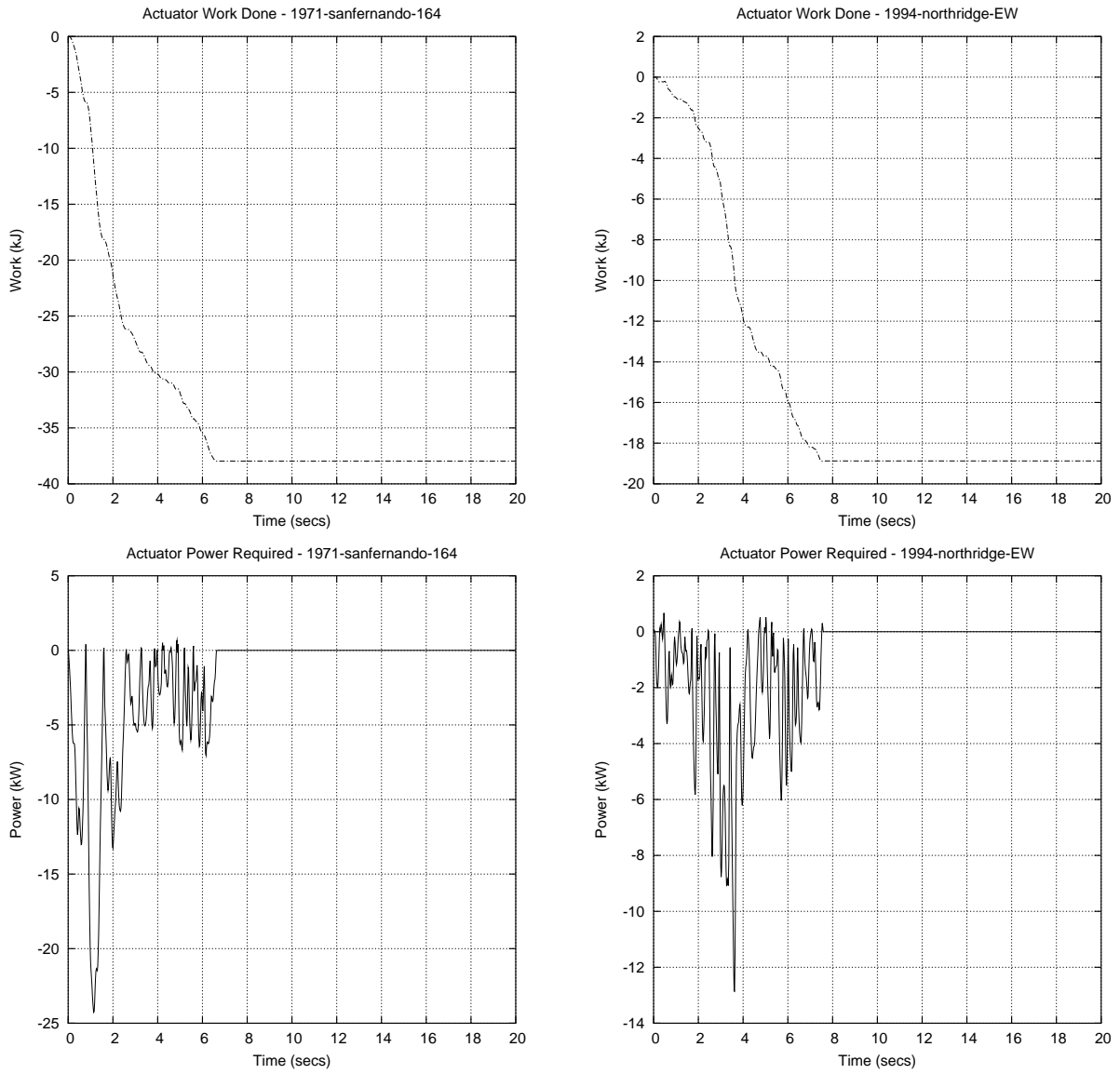
Figure 3.21: Design Case 2. LDBI+CKBB design subject to severe ground excitations: 1971 San Fernando and 1994 Northridge. The upper graphs show actuator work done (kJ) versus time (sec). The lower graphs show power requirements (kW) versus time (sec).
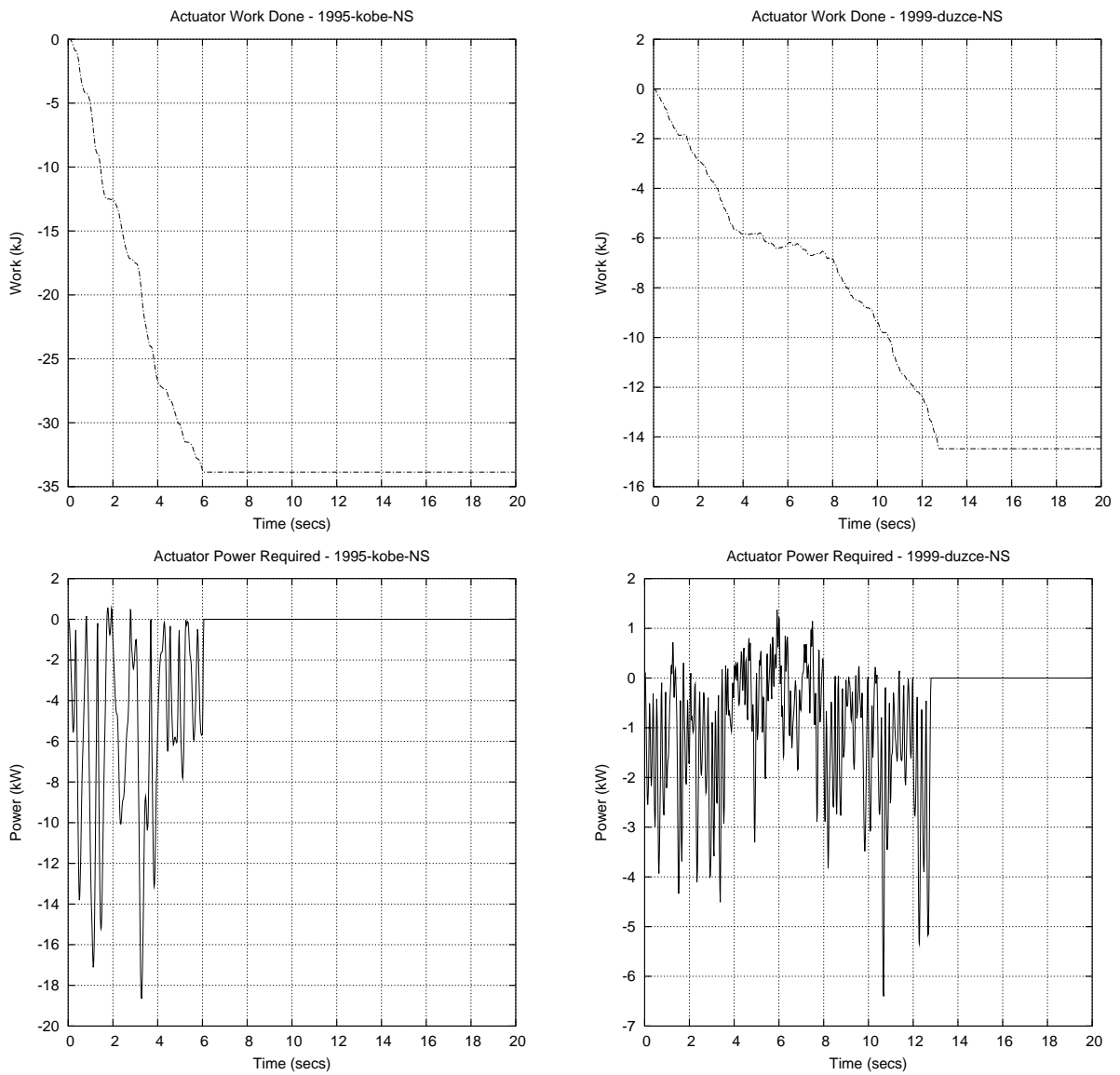
Figure 3.22: Design Case 2. LDBI+CKBB design subject to severe ground excitations: 1995 Kobe and 1999 Duzce. The upper graphs show actuator work done (kJ) versus time (sec). The lower graphs show power requirements (kW) versus time (sec).
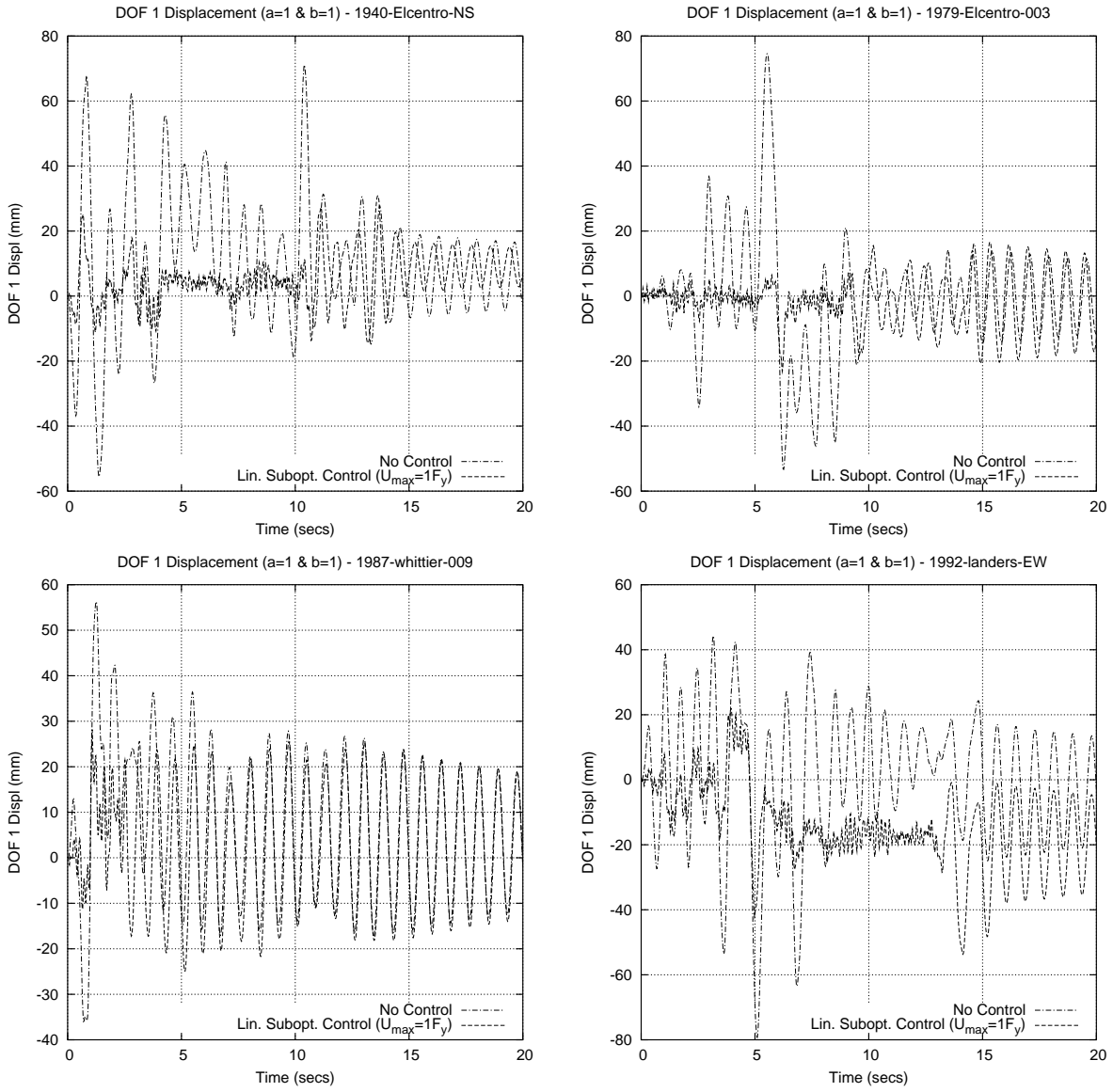
Figure 3.23: Design Case 3. HDBI and HDBI+CKBB designs subject to moderate ground excitations: 1940 El Centro, 1979 El Centro, 1987 Whittier, 1992 Landers. Base isolator drift (mm) versus time (sec).
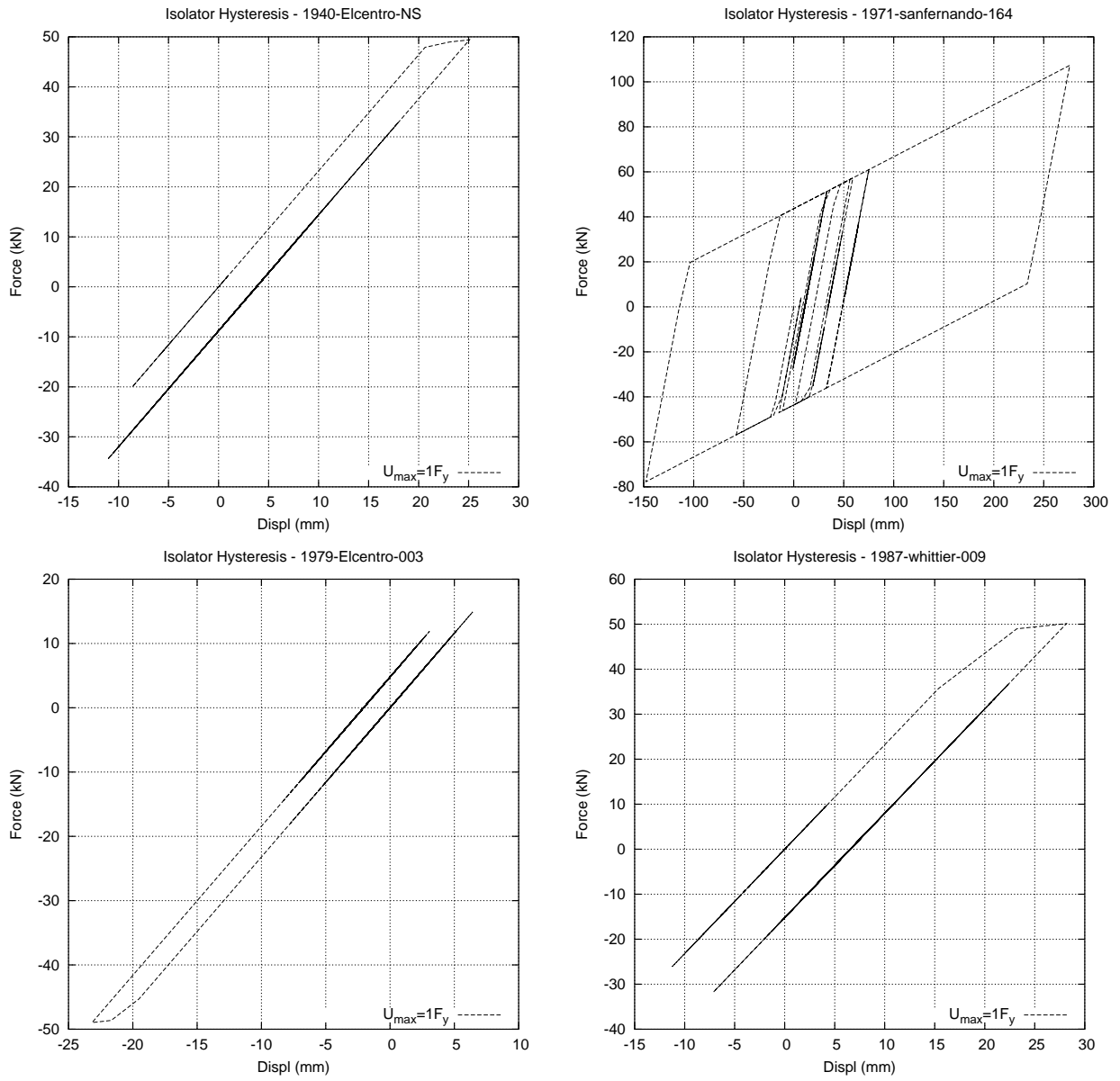
Figure 3.24: Design Case 3. HDBI+CKBB design subject to moderate ground excitations: 1940 El Centro, 1979 El Centro, 1987 Whittier, 1992 Landers. Force-displacement hysteresis curves.
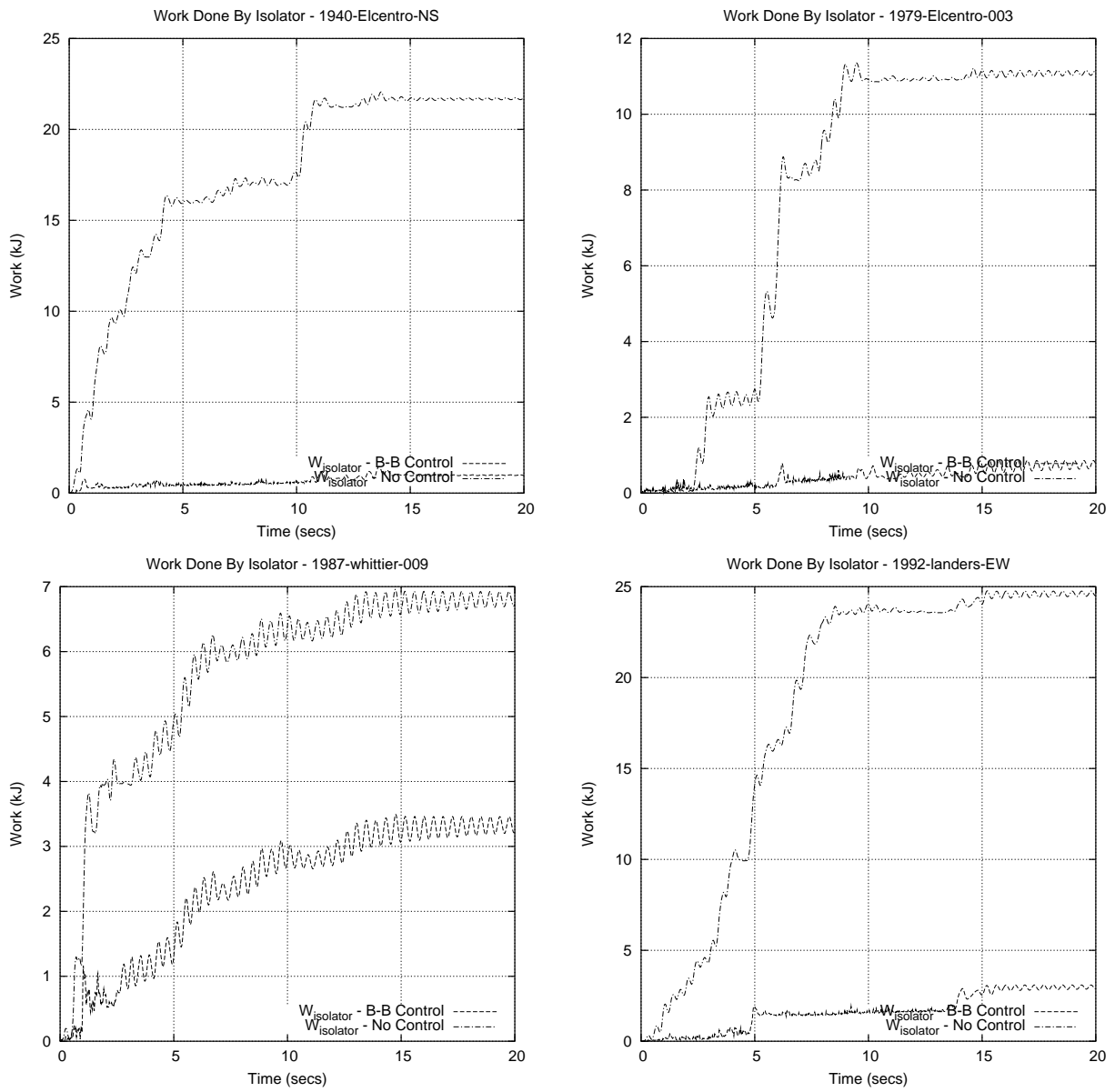
Figure 3.25: Design Case 3. HDBI and HDBI+CKBB designs subject to moderate ground excitations: 1940 El Centro, 1979 El Centro, 1987 Whittier, 1992 Landers. Comparison of base isolator work done (kJ) versus time (sec).
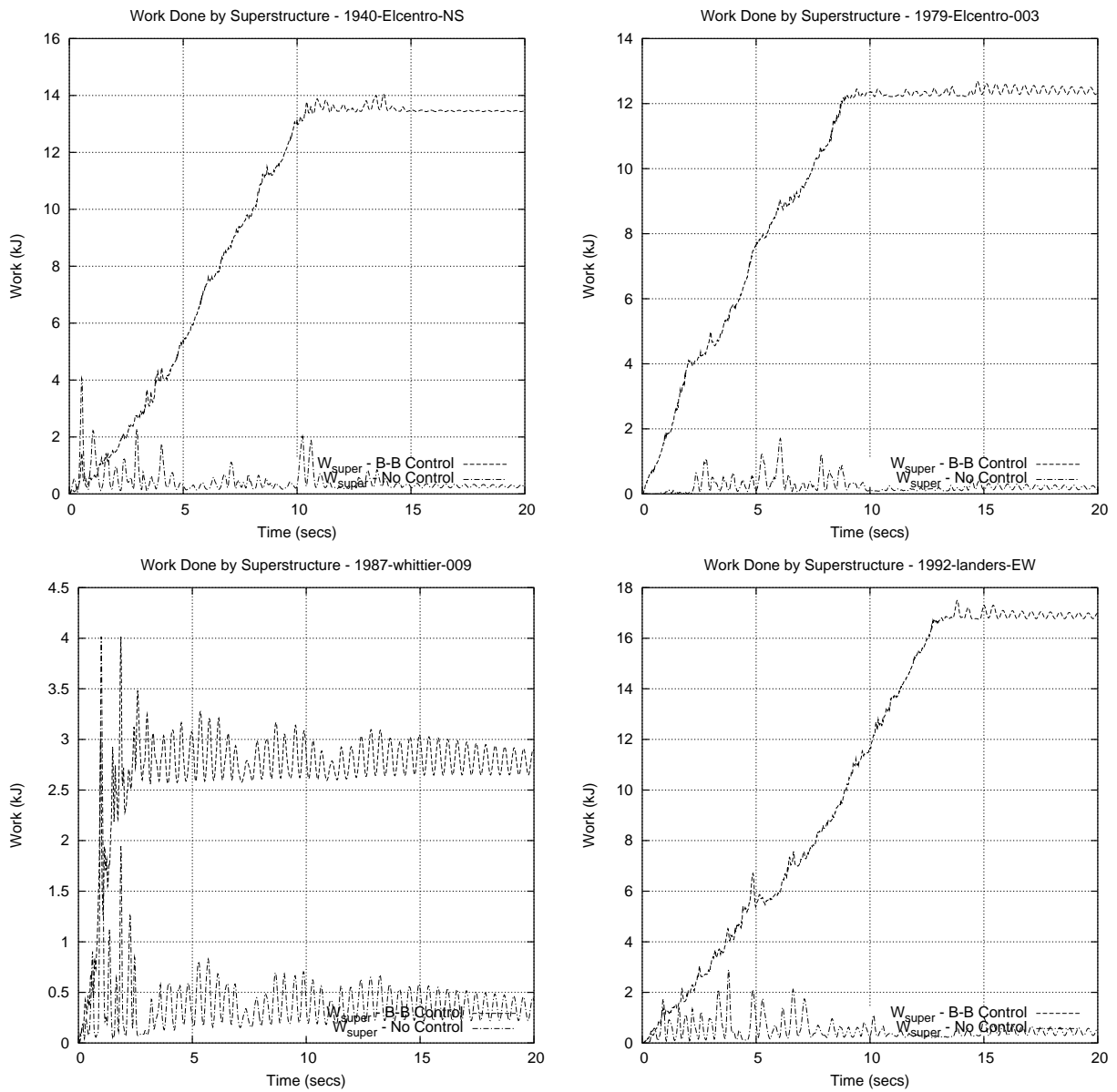
Figure 3.26: Design Case 3. HDBI and HDBI+CKBB designs subject to moderate excitations: 1940 El Centro, 1979 El Centro, 1987 Whittier, 1992 Landers. Comparison of superstructure work done (kJ) versus time (sec).

50
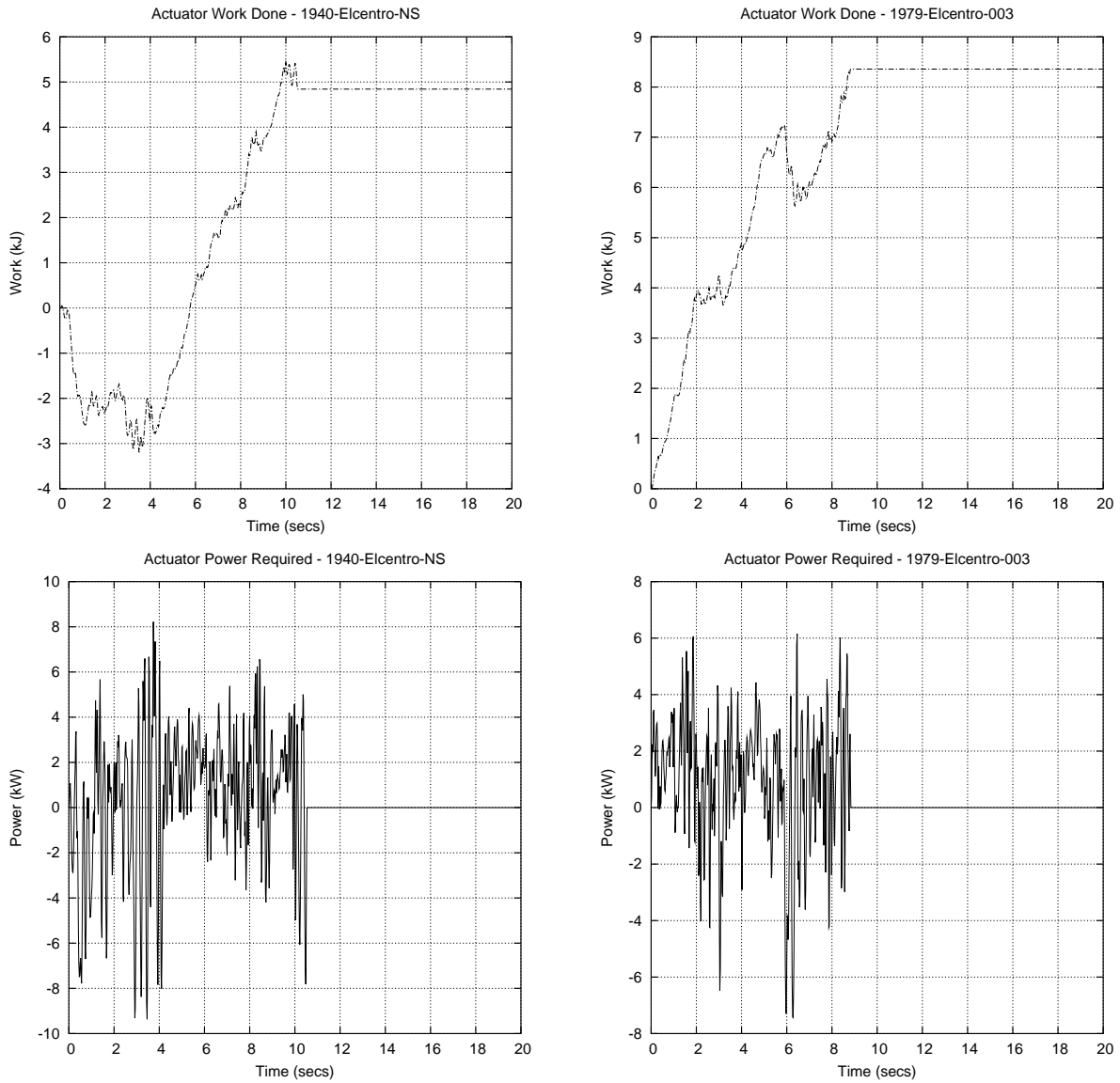
Figure 3.27: Design Case 3. HDBI+CKBB design subject to moderate ground excitations: 1940 El Centro and 1979 El Centro. The upper graphs show actuator work done (kJ) versus time (sec). The lower graphs show power requirements (kW) versus time (sec).
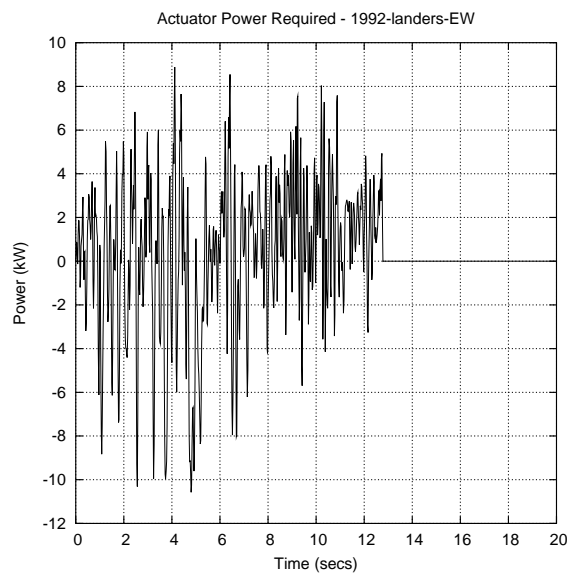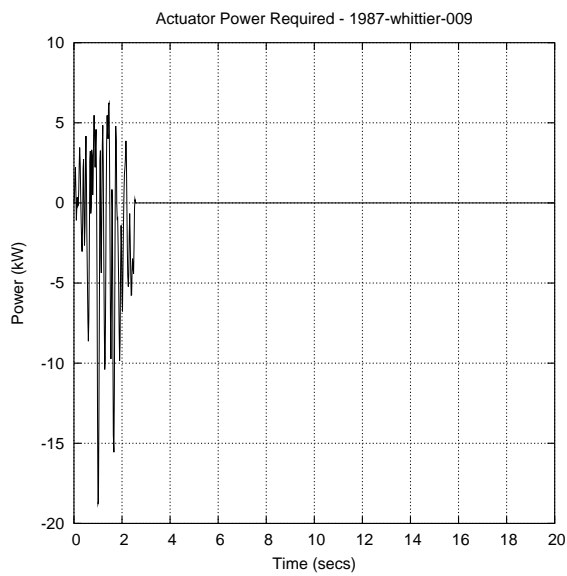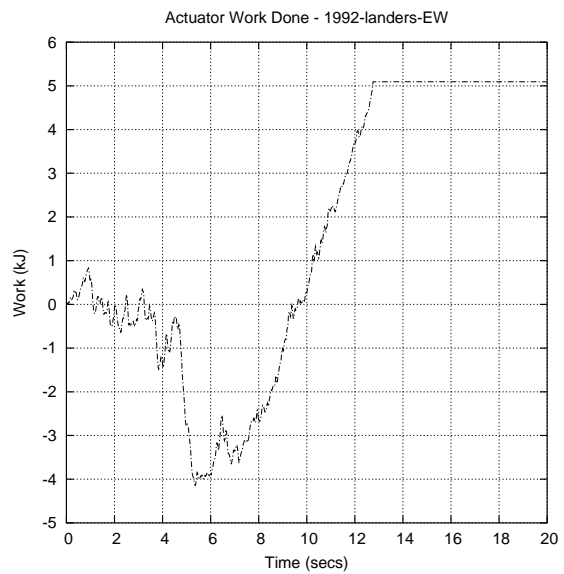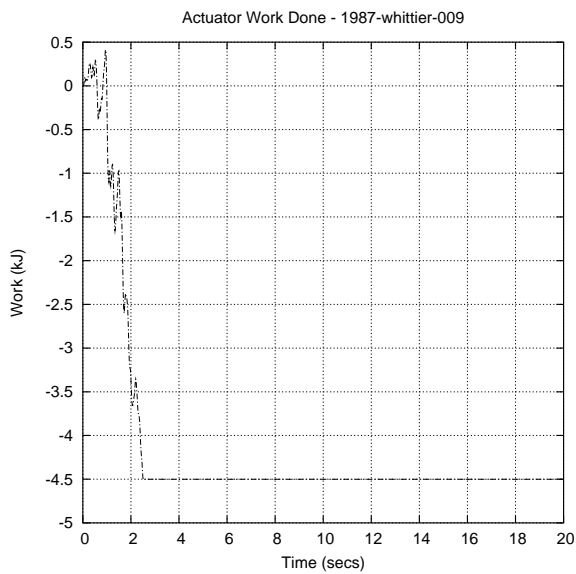
Figure 3.28: Design Case 3. HDBI+CKBB design subject to moderate ground excitations: 1987 Whittier and 1992 Landers. The upper graphs show actuator work done (kJ) versus time (sec). The lower graphs show power requirements (kW) versus time (sec).
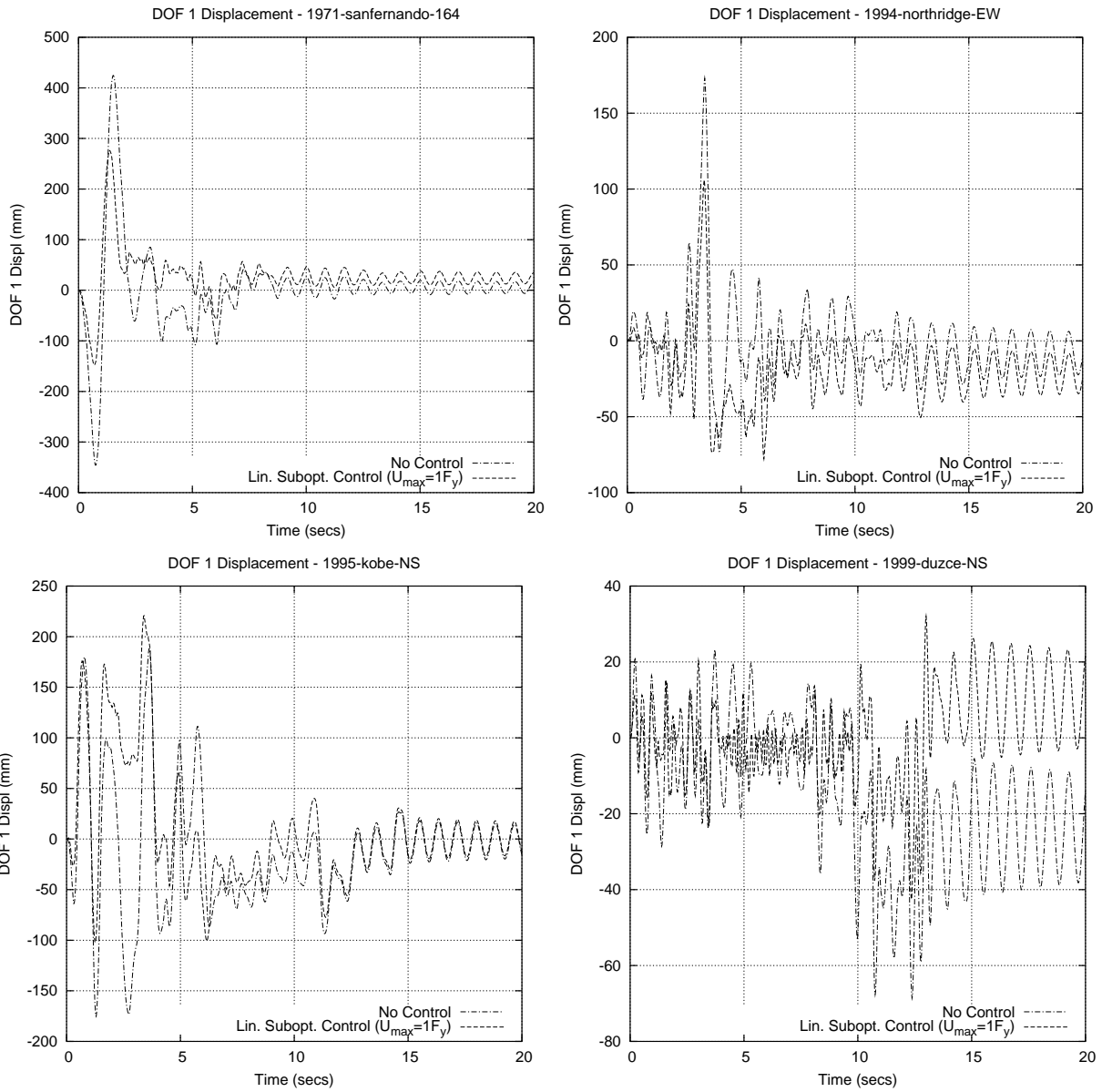
Figure 3.29: Design Case 4. HDBI and HDBI+CKBB designs subject to severe ground excitations: 1971 San Fernando, 1994 Northridge, 1995 Kobe, 1999 Duzce. Base isolator drift (mm) versus time (sec).

53
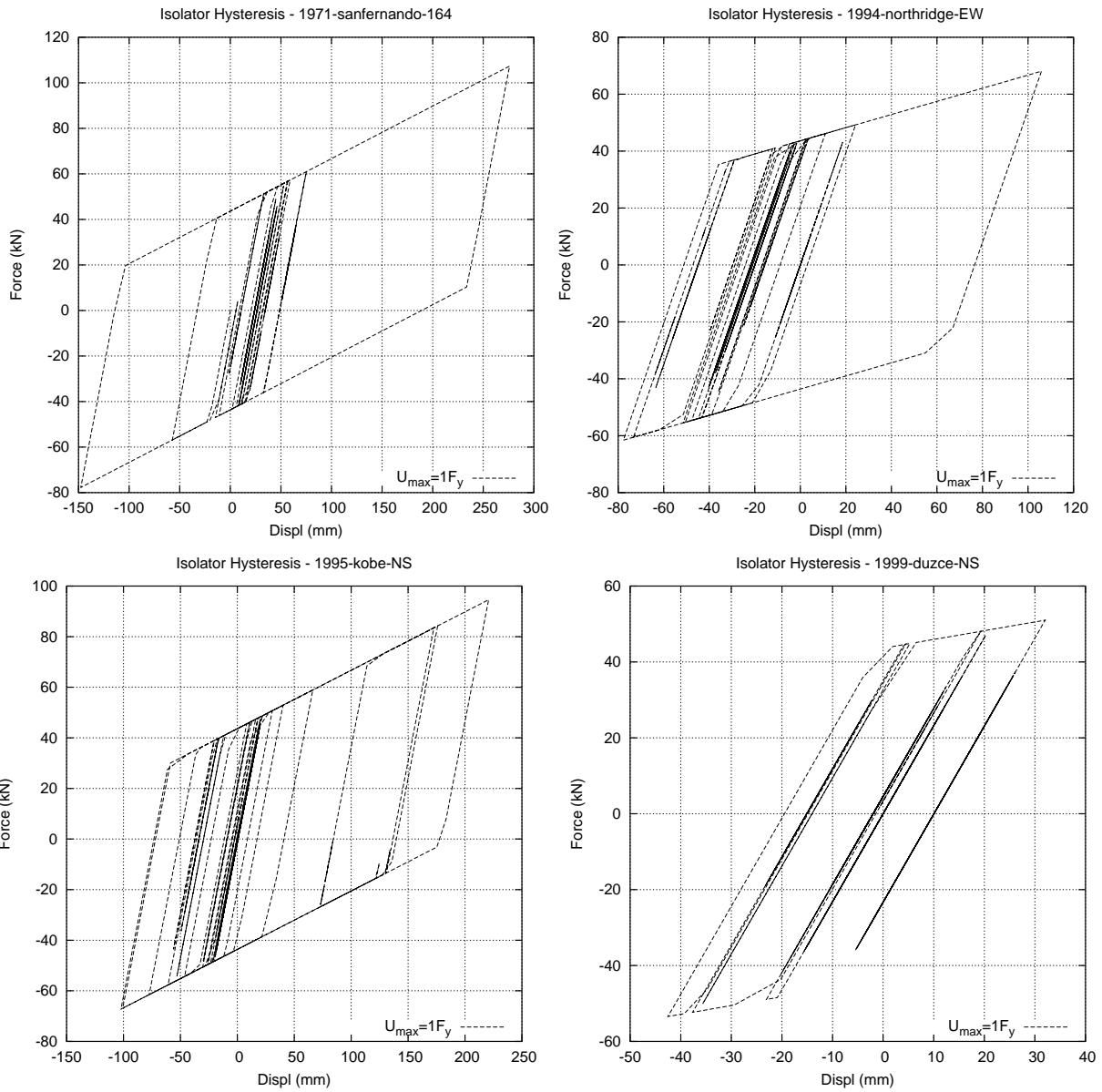
Figure 3.30: Design Case 4. HDBI+CKBB design subject to severe ground excitations: 1971 San Fernando, 1994 Northridge, 1995 Kobe, 1999 Duzce. Force-displacement hysteresis curves.
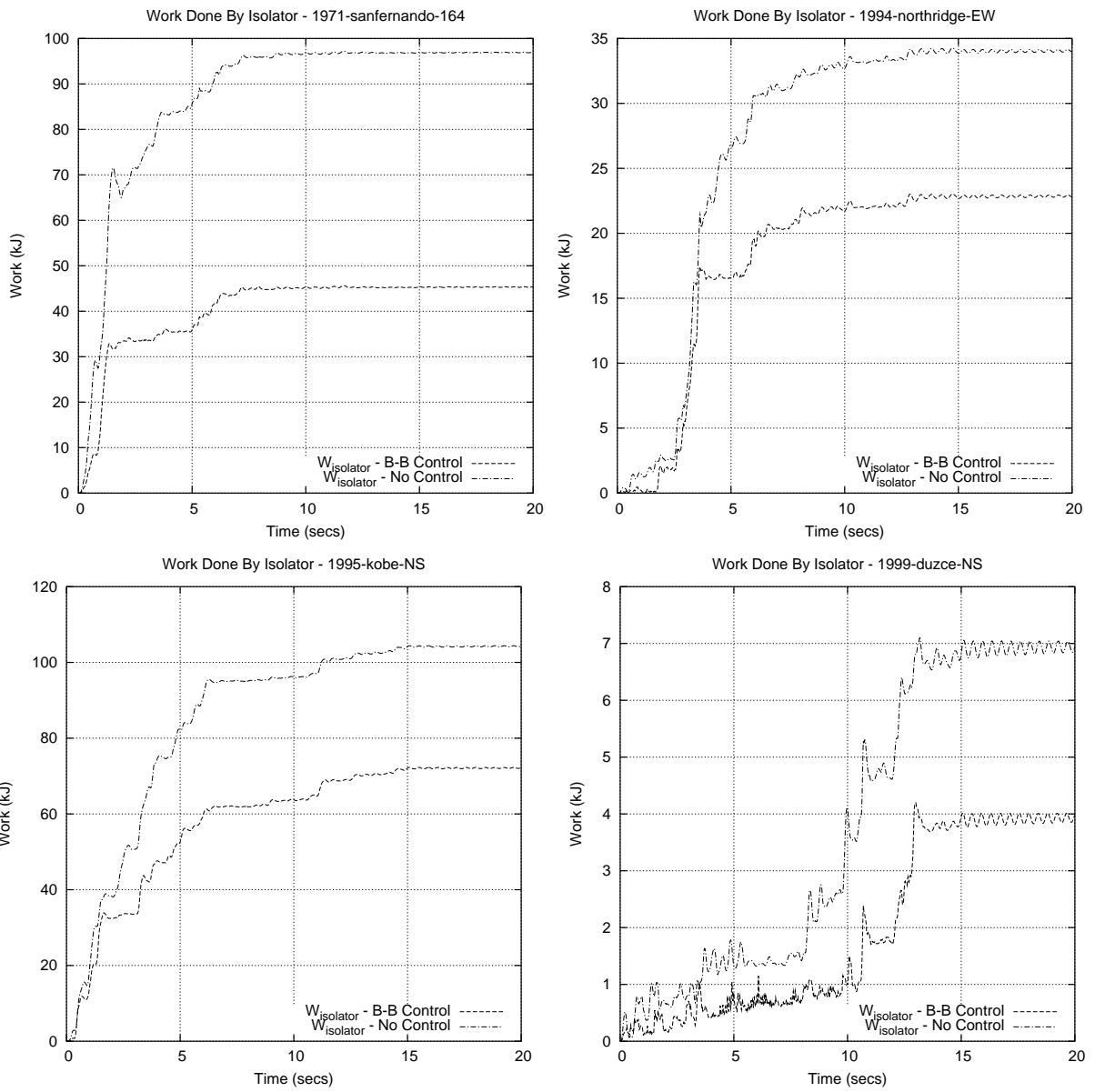
Figure 3.31: Design Case 4. HDBI and HDBI+CKBB designs subject to severe ground excitations: 1971 San Fernando, 1994 Northridge, 1995 Kobe, 1999 Duzce. Comparison of base isolator work done (kJ) versus time (sec).

55
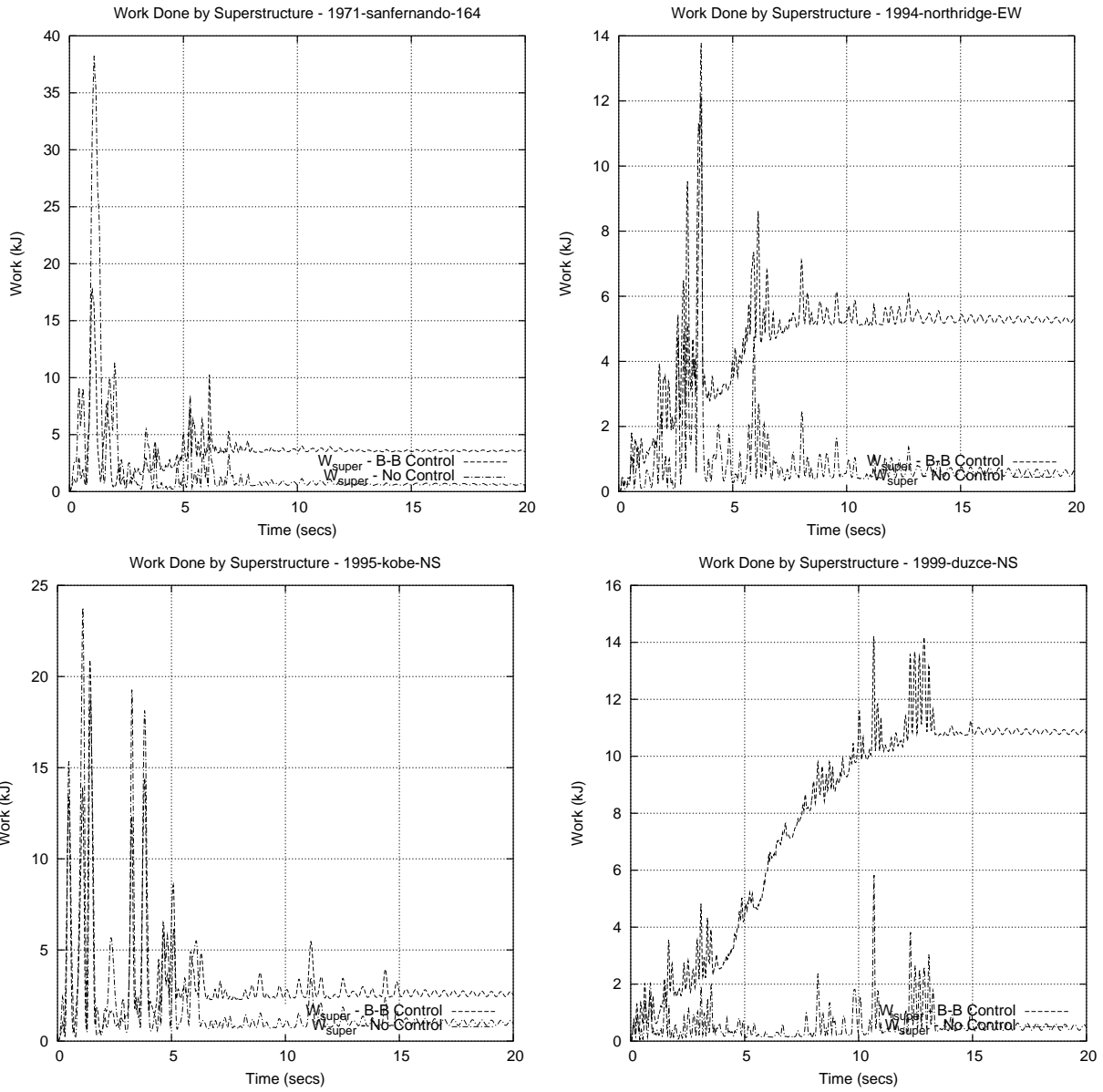
Figure 3.32: Design Case 4. HDBI and HDBI+CKBB designs subject to severe ground excitations: 1971 San Fernando, 1994 Northridge, 1995 Kobe, 1999 Duzc. Comparison of superstructure work done (kJ) versus time (sec).
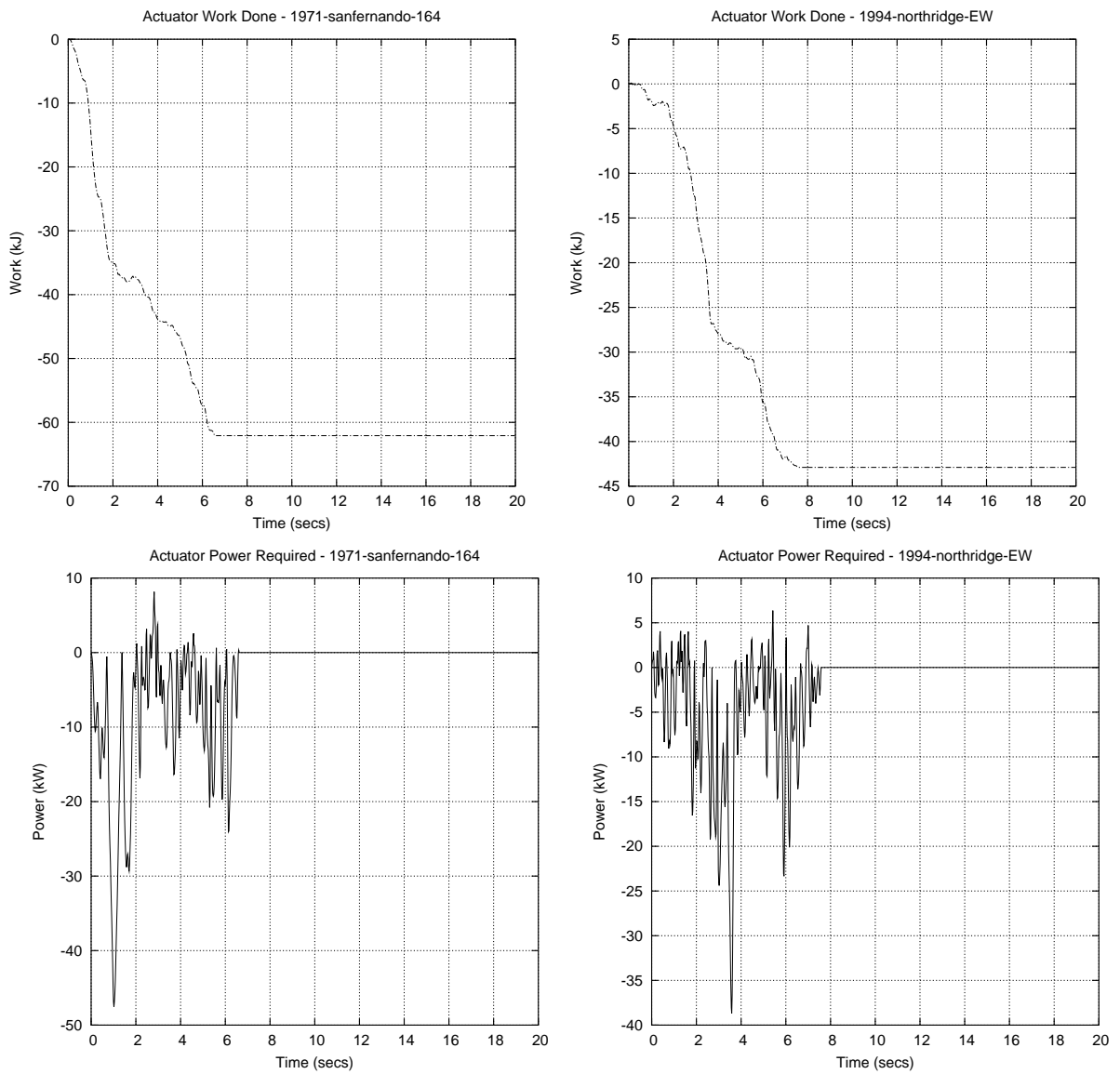
Figure 3.33: Design Case 4. HDBI+CKBB design subject to severe ground excitations: 1971 San Fernando, 1994 Northridge. The upper graphs show actuator work done (kJ) versus time (sec). The lower graphs show power requirements (kW) versus time (sec).

57
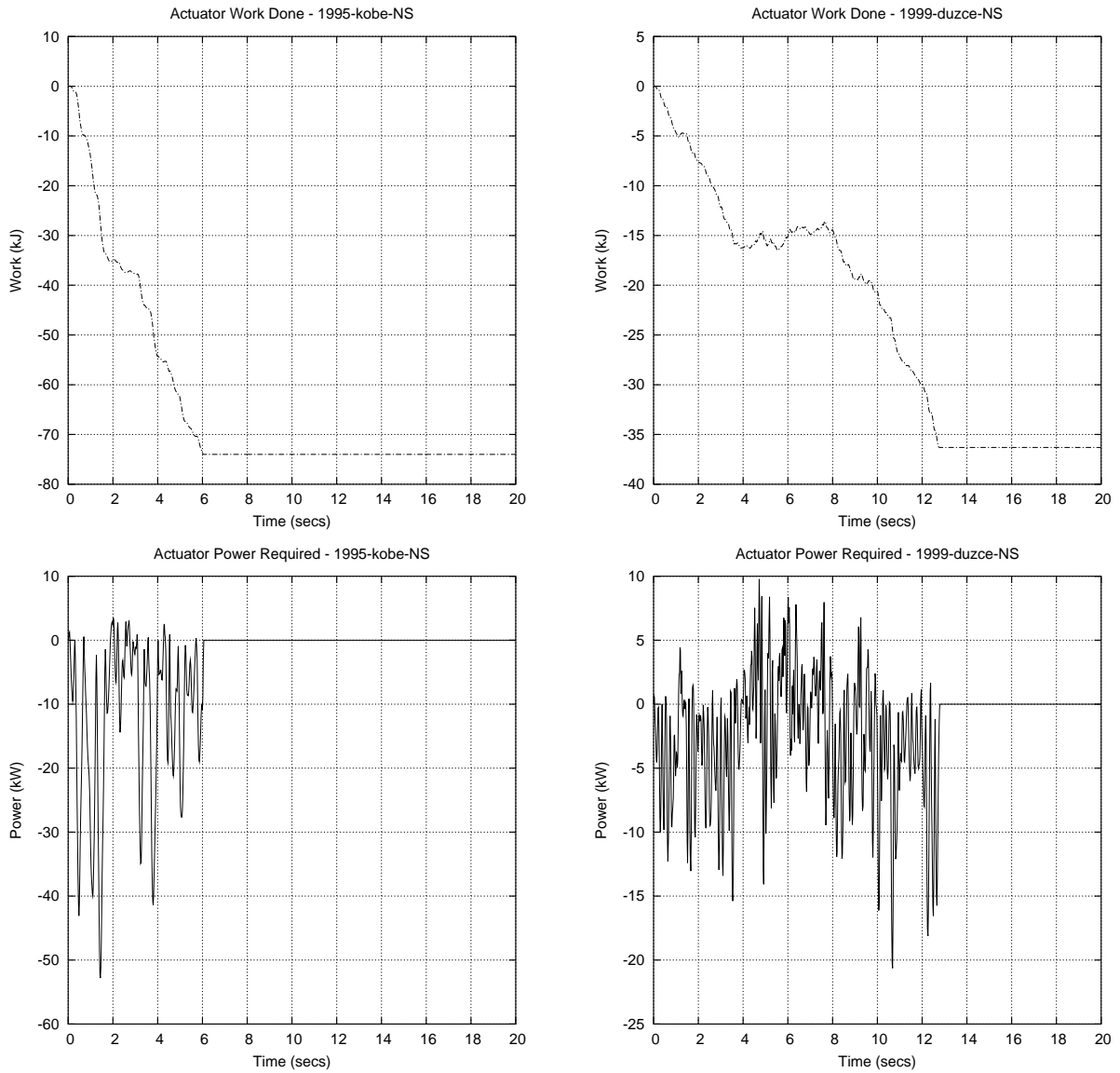
Figure 3.34: Design Case 4. HDBI+CKBB design subject to severe ground excitations: 1995 Kobe and 1999 Duzce. The upper graphs show actuator work done (kJ) versus time (sec). The lower graphs show power requirements (kW) versus time (sec).

58

Chapter 4

State-of-the-Art Actuator Technology

4.1　Introduction

The active control of Civil Engineering structures with actuators generally requires large control forces (on the order of a meganewton) and for seismic excitations, response times on the order of milliseconds. There are hydraulic, electromechanical, and electromagnetic devices capable of delivering such a large force, but they also have a high energy demand. Indeed, high forces coupled with constraints on energy demand is very difficult to achieve [11]. In an effort to mitigate these limitations, considerable research is underway to develop new, large, controllable force capacity actuators that have a low energy demand.

Instead of trying to reduce peak values of system response through the application of large actuator forces, semi-active control devices impart forces to change properties of the system (e.g., stiffness, damping). The power requirements for semi-active control are much less than for actuator enabled control. In fact, many semi-active control devices operate on battery power, which is critical during ground excitations when the power source to the structure may fail. Spencer and Sain [45] report that when semi-active damping systems are implemented appropriately, they have the potential to perform significantly better than passive devices, even surpassing the performance of fully active systems. Thus, semi-active control devices offer the possiblity of effective response reduction during a wide array of ground excitations.

In this section, we review technologies for active and semi-active control, including material-based actuators suitable for controlling Civil Engineering structures. A summary of key actuator characteristics is shown in Table 4.1.

Actuator Type	Peak Force	Response Time	Power Requirements
Hydraulic	meganewtons	$\sim$10-100 ms	high
Electromechanical	$\sim$600 kNs	tenths of secs	high
Electromagnetic	several kNs	milliseconds	low
Variable Orifice Dampers	$\sim$10-30 kNs	milliseconds	$\sim$50W
Variable Stiffness Damper	$\sim$8-10 kNs +	milliseconds	low
Piezoelectric Actuators	$\sim$20 kNs	milliseconds	$\sim$1000 V
Smart TMDs	$\sim$25 kNs + ($\propto$mass x accel.)	milliseconds	low
MR Actuators	$\sim$200 kNs +	milliseconds	$\sim$50W $\sim$12-24 V $\sim$1-2 A

Table 4.1: Summary of Characteristics of Active/Semiactive Control System Actuators

4.2   Active Control System Actuators

An active control system is one in which an external source powers control actuator(s) that apply forces to the structure in a prescribed manner. These forces can be used to both add and dissipate energy in the structure. Since an active control system can add mechanical energy to the structure, this type of system has the possibility of destabilizing the structure. The energy stability theorem of bounded energy input results in bounded energy output is violated. Examples of active control system actuators fall into the categories of hydraulic, electromechanical, and electromagnetic devices.

Hydraulic Actuators. Hydraulic mechanisms force fluid in or out of a cylinder through an orifice to maintain a certain pressure on the face of a piston head. Precise control movement and force can be achieved with a suitable control system. Dorey and Moore [12] points out that hydraulic mechanisms can produce forces on the order of meganewtons. However, the disadvantages of hydraulic mechanisms are the requirements for fluid storage system, complex valves and pumps are required to regulate the fluid flow and pressure, and that seals require continuous maintenance.

Electromechanical Actuators. Electromechanical actuators generate force by moving a piston with a gear mechanism that is driven by an electric motor. The force is controlled by adjusting the power input to the motor. Response time is high, on the order of tenths of seconds. Electric actuators rated for 600 kN of force are commercial available. There are several manufacturers of linear electromechanical actuators. One such manufacturer is Raco (www.raco.de). Connor [11] notes that because electro-mechanical actuators are composed of many parts that are in contact with each other, there is a high risk of breakdown.

4.3 Semi-Active Control System Actuators

Semi-active control mechanisms have a low ratio of energy demand to force output, and according to presently accepted definitions, a semiactive control device is one that cannot inject mechanical energy into the controlled structural system, i.e., semiactive devices act as energy dissipating mechanisms according to Spencer and Sain [45]. Thus, unlike active control mechanisms, semi-active control mechanisms do not have the potential to destabilize the structural system in a bounded input/bounded output sense. Examples of semi-active control system actuators fall into the categories of adaptive configuration-based actuators and controllable fluid-based actuators. Adaptive configuration-based actuators have the characteristic of being able to generate a large force by changing their physical makeup while controllable fluid-based actuators contain a fluid that is characterized by it's ability to change to a semisolid in milliseconds. Examples of adaptive configuration-based actuators include variable orifice dampers, variable stiffness devices, piezoelectric actuators, and smart tuned mass dampers (STMDs). Examples of controllable fluid-based actuators include electroheological (ER) and magnetorheological (MR) based actuators.

Electromagnetic Actuators. Electromagnetic force mechanisms are based on the interaction between the magnetic field generated by the stationary field magnet and the current in the driving coil. A driving coil is attached to the piston, which translates with respect to the housing. Since electromagnetic actuators are driven by magnetic forces, they do not require mechanical contact and are therefore theoretically more reliable than hydraulic or electromechanical actuators. According to Connor [11], electromagnetic actuators with a force capacity up to several kilonewtons are commercially available and the force response time is on the order of milliseconds. Research and development of larger capacity actuators is currently underway. Connor [11] also points out that Chaniotakis et al. at the Massachusetts Institute of Technology is currently developing a large-scale electromagnetic actuator that may have full-scale applications. Disadvantages of electromagnetic actuator technology is a commercially available product in the meganewton range is still in the research and development phase, and probably the voltage and current requirements for such a actuator can not be satisfied with conventional electrical power supply technology.

Variable Orifice Dampers. Variable orifice dampers use a control valve to alter the resistance to flow of a conventional hydraulic fluid damper. The valve opening adjusts according to force demand that is determined by a feedback control algorithm. Since the valve motion is perpendicular to the flow, the force required to adjust the valve position is small and energy demand is low (usually on the order of

30-50 watts) according to Connor [11] and Spencer and Nagarajaiah [44]. Variable orifice dampers were implemented by Kurata et al. [27] in a large-scale, three-story frame structure and Sack and Patten [40] and Patten et al. [35] developed a variable orifice damper and Patten et al. [36] installed a hydraulic actuator with a controllable orifice on a bridge in Oklahoma.

Variable Stiffness Devices. Kobori et al. [26] conceived of using a full-scale variable orifice damper in on-off mode – a high stiffness device due to the lack of compressibility of hydraulic fluid when the valve is closed or a device with no stiffness when the valve is open – as a semiactive variable stiffness system. However, this system was not able to vary stiffness continuously from one state to another. However, according to Spencer and Nagarajaiah [44], Nagarajaiah has developed a semiactive variable-stiffness device (SAIVS) (U.S. Patient No. 6,098,969). Nagarajaiah and Mate [33] has shown in a scaled structural model that SAIVS can effectively smoothly vary the stiffness of a structure and produce a nonresonant system.

Piezoelectric Actuators. Piezoelectric actuators are fabricated with piezoceramic block-type elements or piezopolymer films. When a voltage is applied, these piezoceramic/piezopolymer materials extend or contract. When these materials are attached to a surface which restrains their motion and a voltage is applied, contact forces between the object and the restraining medium are produced. Two config-urations are available. According to Connor [11], one configuration produced by Kinetic Ceramics, Inc. (www.kineticceramics.com) used piezoceramic wafers stacked vertically and produces a maximum force of 20 kN with a response time of several milliseconds. A second configuration produced by Active Control Experts (www.acx.com) uses piezoceramic wafers distributed over an area in a regular pattern produces a maximum force of 500 N at 200 volts with millisecond response.

Smart Tuned Mass Dampers (STMDs) Conventional tuned mass dampers (TMDs) are not adaptable due to their fixed design. An alternative is the STMD that continuously retunes its frequency due to real time control thus making it robust to changes in building stiffness and damping. Nagarajaish and Varadarajan [?] have shown the effectiveness of the SAIVS device to act as an integral part of the STMD system by controlling a small-scale three story structural model. Varadarajan and Nagarajaish [54] stud-ied the response control of an analytical model of a 76-story concrete office tower. The SAIVS device was part of a 500 ton STMD system that was demonstrated to substantially reduce the building when compared to a TMD system and reduce a similar response to a active mass damper system (AMD) sys-tem based on a LQG controller, but with a magnitude less power consumption comparable to active tuned mass dampers, but with a order of magnitude less power consumption. STMD systems have also been
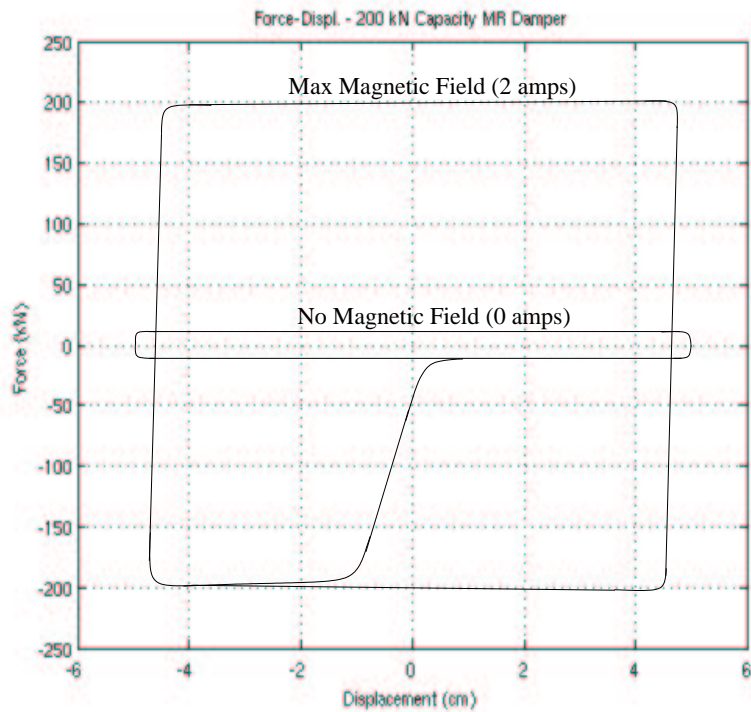
Figure 4.1: Hysteresis for 200-kN MR Damper [44]

proposed based on controllable tuned sloshing dampers (CTSDs). Tuned sloshing dampers (TSDs) use the liquid sloshing in a tank to add damping to the structure. Lou et al. [29] have proposed a semiactive CTSD device in which the length of the sloshing tank is altered to change the properties of the device.

Electrorheological (ER) and Magnetorheological (MR) Based Actuators. The common characteristic of both ER and MR fluids is their ability to change from free-flowing (in this state the fluid may be modeled as Newtonian) to a semisolid with a controllable yield strength in milliseconds. However, only MR fluids have been shown to be tractable for civil engineering applications according to Spencer and Sain [45]. MR fluids typically consist of micronsized, magnetically polarizable particles dispersed in a carrier medium such as mineral or silicone oil, and Spencer and Nagarajaiah [44] that MR fluid actuators have been shown to be readily controlled with low power (e.g. less than 50 W), low voltage (e.g. $\sim$12-24 V), and a power supply only outputting $\sim$ 1-2 A. Simulations and laboratory model experiments [13, 14, 30, 38, 45, 46, 43, 59, 60] have shown that MR significantly outperforms comparable passive damping configurations, and requires only a fraction of the input power needed by active controllers. Carlson and Spencer [10] and Spencer et al. [47] have studied a 200-kN capacity MR damper which may be used for full-scale applications. Figure 4.1 shows the measured force-displacement loops for this damper [44].

63

Chapter 5

Conclusions

5.1 Summary and Conclusions

Summary. The objectives of this study have been two-fold. First, using the metrics of energy- and power-balance assessment, and peak base drifts, we have identified scenarios when constant stiffness bang-bang (CKBB) control can benefit base isolation. Energy-based metrics are useful because they provides a means for quantitatively estimating the capacity of a structure to: (1) Resist forces elastically, (2) Dissipate energy associated with damping mechanisms, and (3) Support cyclic nonlinear deformations in key structural elements without a premature loss in strength. Power-balance analysis extends energy-based analysis to include the external influence of actuator control on system response. Evaluation of the second objective boils down to a question of technology assessment – can present-day actuator technologies deliver the force/reach implied by the simulations computed in this study?

The numerical experiments have been based on time-history responses of a six-DOF mass-damping-spring system proportioned according to two design philosophies: (1) Low-damping base isolation (LDBI) for moderate ground motions (i.e., "size and characteristic" of the 1940 El Centro earthquake, PGA~0.35g), and (2) High-damping base isolation (HDBI) for maximum credible ground motions (e.g, 1994 Northridge earthquake, PGA~1.225g). For each design case, system responses have been computed for ensembles of ground motion scaled to moderate and severe intensity. Improvements in system response due to control are benchmarked against the system responses resulting from LDBI/HDBI base isolation alone, and systematic variations in ground motion intensity and the details of design methodology.

Conclusions. With respect to the time-history responses and associated energy- and power-balance analyses, the conclusions of this study are as follows:

1. The numerical experiments indicate that a judicious application of CKBB control can lead to significant improvements in system response compared to those due to base isolation alone. For scenarios of moderate earthquake attack, system responses due to base isolation alone are satisfactory – this is, after all, the purpose of base isolation mechanisms. CKBB control is most effective in countering extreme values of system performance when base isolated systems are subject to severe ground motion attack. The statistics of performance improvement in peak values of base drift, reductions in energy demands on the base isolator, and actuator power demands are well documented in Section 3.4. Notice that in all cases, the addition of CKBB control reduces the amount of work done by the base isolator. This observation validates the theoretical formulation for energy-based control.

2. However, is it equally evident that too much control, whether it be through magnitude of the control force or duration of application, can deteriorate performance. Rather than extract energy from the influence of external loads, the situation of "too much" control can feed energy into the system. The latter scenario is most likely to occur after ground motions have ceased and/or during periods of low input energy per unit time. This conclusion points to a strong need for development of a time-adaptive bang-bang control strategy that uses earthquake energy input to navigate trade-offs between work done by the base isolator, superstructure, and actuator.

3. The numerical experiments have exposed an apparent dilemma – sometimes reductions in peak values of base drift are accompanied by actuator actions that actually feed energy into the system. As a first step toward understanding this phenomenon, Figure 3.10 shows "work done by the actuator" versus "Arias Intensity (m/sec)" for the system responses scaled to moderate and severe ground shaking intensity. Other than noting that "work done by the actuator" is smaller for design cases 2 and 1 than design cases 4 and 3, respectively, it is difficult to identify from Figure 3.10 cause-and-effect relationships that have practical meaning. Notice, however, that if we plot "work done by the actuator" versus "ground motion input energy (AI)/per unit time," as shown in Figure 3.11, the eight system responses for moderate ground shaking separate into two groups. The smaller group of three responses corresponds to the three system reponses where actuator input energy is positive. We already know from our previous work that the actuator will input energy into the system once the ground motion has stopped. This observation suggests that input energy may also be positive for ground motions where "ground motion input energy (AI)/per unit time" is small.

4. Further work is need to identify trends between "work done by the actuator" and "magnitude of
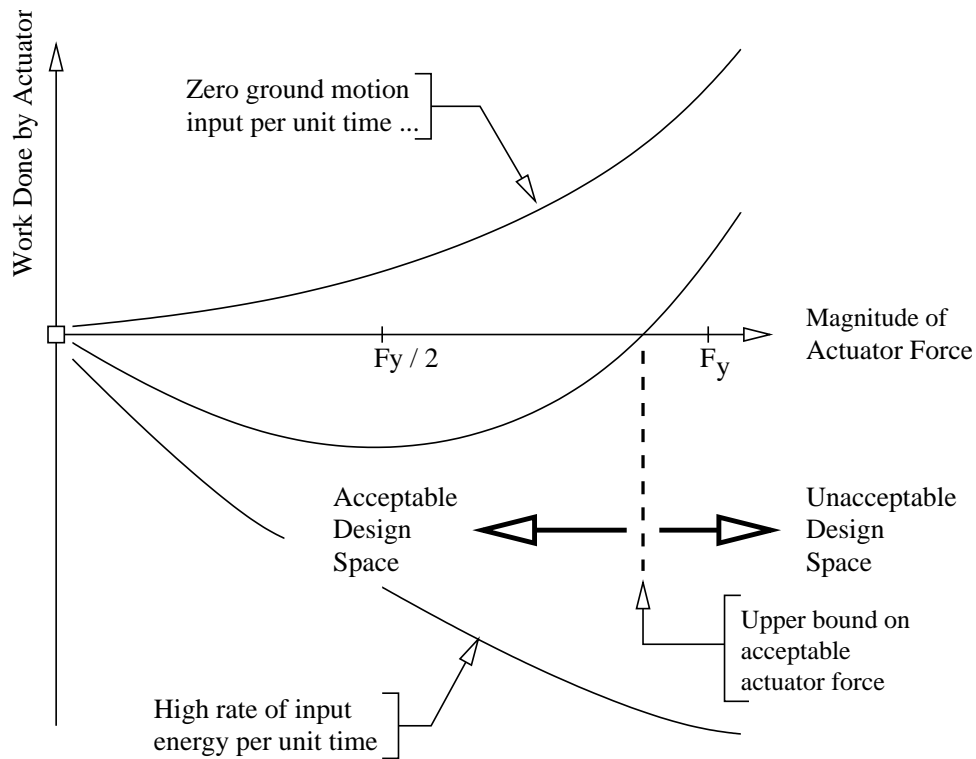
Figure 5.1: "Work done by actuator" (kJ) versus "Magnitude of Actuator Force" for Low, Medium, High Contours of Energy Input/per unit time

the actuator force" for contours of constant input energy per unit time. If the goal of the active control mechanism is to extract energy from the system response, while at the same time also decreasing displacements, then we surmise that connectivity among these relationships might be as shown in Figure 5.1. Design considerations dictate that nomatter how high the rate of energy input becomes, the actuator force should never exceed the lateral yield force of the base isolation system. Appropriate maximum values of actuator force for moderate rates of input energy might be considerably less than the yield force, but would move toward the lateral yield force of the base isolation system as the rate of input energy increases. Conversely, if the actuator force is too small, then the actuator mechanism will be ineffective. Further work is needed to identify the existence of an "upper bound on acceptable actuator force" and to connect this bound to a time-adaptive strategy for bang-bang control.

With respect to actuator technology assessment, the conclusions of this study are:

1. For our scaled model, actuators were modeled as having a maximum peak force of 14.46 kN and 43.39 kN. For a similar full scale structure, depending on the scaling factor, Table 4.1 shows that

66

several semiactive actuators that are currently being produced that would be able to generate the required force within milliseconds with very little power (some even operating with batteries). In the event of a large scaling factor, the required actuator forces can be generated with parallel configurations of dampers based on the current technology shown in Table 4.1.

5.2   Acknowledgements

Bibliography

[1] AASHTO. *Guide Specifications for Seismic Isolation Design*. 1991.

[2] Andriono T., Carr A.J. A Simplified Earthquake Resistant Design Method for Base Isolated MultiStorey Buildings. *Bulletin of the New Zealand National Society for Earthquake Engineering*, 24(3):238–250, September 1991.

[3] Andriono T., Carr A.J. Reduction and Distribution of Lateral Seismic Forces on Base Isolated Mutli-Storey Structures. *Bulletin of the New Zealand National Society for Earthquake Engineering*, 24(3):225–237, September 1991.

[4] Arias A. *A Measure of Earthquake Intensity in Seismic Design for Nuclear Power Plants*. MIT Press, 1970. Hansen R., ed.

[5] Austin M. A., and Lin W. J. Energy-Balance Assessment of Isolated Structures. *Journal of Engineering Mechanics*, 130(3):347–358, 2003.

[6] Austin M. A., Lin W. J., and Chen X. G. Structural Matrix Computations with Units. *Journal of Computing in Civil Engineering*, 14(3):174–182, 2000.

[7] Austin M. A., Chen X. G., Lin W-J. ALADDIN: A Computational Toolkit for Interactive Engineering Matrix and Finite Element Analysis. Technical Report TR95-74, Institute for Systems Research, University of Maryland, College Park, December 1995.

[8] Austin M. A., Pister K. S., Mahin S. A. A Methodology for the Probabilistic Limit States Design of Earthquake Resistant Structures. *Journal of the Structural Division, ASCE*, 113(8):1642–1659, August 1987.

[9] Austin M. A., Pister K. S., Mahin S. A. Probabilistic Limit States Design of Moment Resistant Frames Under Seismic Loading. *Journal of the Structural Division, ASCE*, 113(8):1660–1677, August 1987.

[10] Carlson, J. D., and Spencer, B. F., Jr. MR Fluid Dampers for Semi-Active Seismic Control. In *Proceeding of 3rd Int. Conference on Vibration Control*, volume III, pages 35–40, 1996.

[11] Connor J.J. *Introduction to Structural Motion Control*. Pearson Education, Inc., 2003.

[12] Dorey, A. P. and Moore, J. H. *Advances in Actuators*. Institute of Physics Publishing, Bristol, England, 1996.

[13] Dyke S. J., Spencer B. F., Jr., Sain M. K., and Carlson, J. D. Modeling and Control of MR Dampers for Seismic Response Reduction. *Smart Mater. Struct.*, 5:565–575, 1996.

[14] Dyke S. J., Spencer B. F., Jr., Sain M. K., and Carlson, J. D. An Experimental Study of MR Dampers for Seismic Protection. *Smart Mater. Struct.*, 7:693–703, 1998.

[15] Earthquake Engineering Research Center, UC Berkeley. Pacific Earthquake Engineering Research (PEER) Strong Motion Database. *http://peer.berkeley.edu/smcat/index.html*.

[16] Fajfar P. Equivalent Ductility Factors, Taking Into Account Low-Cycle Fatigue. *Earthquake Engineering and Structural Dynamics*, 21:837–848, 1992.

[17] Ghobarah A., Ali H.M. Seismic Design of Base-Isolated Highway Bridges utilizing Lead-Rubber Bearings. *Canadian Journal of Civil Engineering*, 17:413–422, 1990.

[18] Hall J. F., Heaton T. H., Halling M. W., and Wald D. J. Near-Source Ground Motion and its Effects on Flexible Buildings. *Earthquake Spectra*, 11(4):569–605, 1995.

[19] Heaton T. H., Hall J. F., Wald D. J., and Halling M. W. Response of High-Rise and Base-Isolated Buildings in a Hypothetical Mw 7.0 Blind Thrust Earthquake. *Science*, 267.

[20] Housner G. W., Bergman L. A., et al. Structural Control: Past, Present, and Future. *Journal of Engineering Mechanics*, 123(9):897–971, 1997.

[21] Housner G.W. Limit Design of Structures to Resist Earthquakes. In *Proceedings of the World Conference on Earthquake Engineering*, Berkeley,California, 1956. Earthquake Engineering Reseach Center.

[22] Housner G.W. Behavior of Structures During Earthquakes. *Journal of the Structural Division, ASCE*, 85(4):109–124, April 1959.

[23] Johnson E. A., Ramallo J. C., Spencer B. F., Jr., and Sain M. K. Intelligent Base Isolation Systems. In *Proceedings of the Second World Conference on Structural Control*, 1998.

[24] Kelly J. M. and Tsai H. Seismic Response of Light Internal Equipment in Base Isolated Structures. Report No. UCB/SESM-84/17, Department of Structural Engineering and Structural Mechanics, Berkeley, CA, September 1984.

[25] Kelly J. M., Leitmann G., and Soldatos A. G. Robust Control of Base-Isolated Structures Under Earthquake Excitation. *Journal of Optimization Theory and Applications*, 53(2):159–180, 1987.

[26] Korbori, T., Takahashi, M., Nasu, T., Niwa, N., and Ogasawara, K. Seismic Response Controlled Structure with Active Variable Stiffness System. *Earthquake Engineering and Structural Dynamics*, 22:925–941, 1993.

[27] Kurata, N., Kobori, T., Takahashi, M., Niwa N., and Kusino H. Shaking Table Experiment of Active Variable Damping System. In *Proceeding of the First World Conference on Structural Control*, volume 2.

[28] Lin W. J. Modern Computational Environments for Seismic Analysis of Highway Bridge Structures, 1997. Doctoral Dissertation.

[29] Lou, J. Y. K., Lutes, L. D., and Li, J. J. Active Tuned Liquid Damper for Structural Control. In *Proceeding of First World Conference on Structural Control*, volume TP1.

[30] Madden G. J., Wongprasert, N., and Symans, M. D. Experimental Verification of Seismic Response of Building Frame with Adaptive Sliding Base-Isolation System. *Journal of Structural Engineering*, 128(8):1037–1045, 2002.

[31] Mayes R.L., Buckle I.G., Kelly T.R., Jones L. AASHTO Seismic Isolation Design Requirements for Highway Bridges. *Journal of the Structural Division, ASCE*, 118(1):284–304, January 1992.

[32] Naeim F. and Kelly J. *Design of Seismic Isolated Structures*. John Wiley and Sons, 1998.

[33] Nagarajaiah, S. and Mate, D. Semi-Active Control of Continuously Variable Stiffness System. In *Proceeding of Second World Conference on Structural Control*, volume 1.

[34] Park J. and Otsuka H. Optimal Yield Level of Bilinear Seismic Isolation Devices. *Earthquake Engineering and Structural Dynamics*, 28.

[35] Patten, W., Sack R., and He, Q. Controlled Semiactive Hydraulic Vibration Absorber for Bridges. *Journal of Structural Engineering*, 122(2):187–192, 1996.

[36] Patten, W., Sun, J., Li, G. Kuehn, J., and Song, G. Field Test of an Intelligent Stiffener for Bridges at the I-35 Walnut Creek Bridge. *Earthquake Engineering and Structural Dynamics*, 28(2):109–126, 1999.

[37] Powell G. H., Allahabadi R. Seismic Damage Prediction by Deterministic Methods: Concepts and Procedures. *Earthquake Engineering and Structural Dynamics*, 16:719–734, 1988.

[38] Ramallo J. C., Johnson E. A., and Spencer B. F., Jr. "Smart" Base Isolation Systems. *Journal of Engineering Mechanics*, 128(10):1088–1099, 2002.

[39] Reinhorn A. M., Soong T. T., and Wen C. Y. Base-isolated Structures with Active Control. In *Proceedings of Pressure Vessels and Piping (PVP) Conference*, volume PVP-127, pages 413–420, 1987.

[40] Sack, R. L. and Patten, W. Semi-Active Hydraulic Structural Control. In *Proceeding of International Workshop on Structural Control*, volume NISTIR 5923. edited by G.W. Housner and S.F. Masri.

[41] Sebastianelli R. R., Jr., and Austin M. A. Computational Assessment of Suboptimal Bang-Bang Control Strategies for Performance-Based Design of Base Isolated Structures. *Journal of Engineering Mechanics in press*.

[42] Skinner R. I., Robinson W. H., and McVerry G. H. *An Introduction to Seismic Isolation*. Wiley Publishing, Chichester, England, 1993.

[43] Spencer B. F., Jr. Civil Engineering Applications of Smart Damping Technology. In *Proceeding of 5th Int. Conference on Vibration Control*, pages 771–782, 2002. Nanjing, China.

[44] Spencer B. F., Jr. and Nagarajaiah S. State of the Art of Structural Control. *Journal of Structural Engineering*, pages 845–856, July 2003.

[45] Spencer, B. F., Jr. and Sain, M. K. Controlling Buildings: A New Frontier in Feedback. *IEEE Control System Magazine*, 17(6):19–35, 1997.

[46] Spencer B. F., Jr., Dyke, S. J., Sain, M. K., and Carlson, J. D. Phenomenological Model of a Magnetorheological Damper. 123(3):230–238, 1997.

[47] Spencer B. F., Jr., Yang, G., Carlson, J. D., Sain, M. K. "Smart" Dampers for Seismic Protection of Structures: A Full-Scale Study. In *Proceeding of Second World Conference on Structural Control*, volume 1, pages 417–426. Wiley, New York, 1999.

[48] *Dynamic Structural Design : An Inverse Approach*. WIT Press, 2000.

[49] Turkington D.H., Carr A.J., Cooke N., and Moss P.J. Design Method for Bridges on Lead-Rubber Bearings. *Journal of the Structural Division, ASCE*, 115(12):3017–3030, December 1989.

[50] Turkington D.H., Carr A.J., Cooke N., and Moss P.J. Seismic Design of Bridges on Lead-Rubber Bearings. *Journal of the Structural Division, ASCE*, 115(12):3000–3016, December 1989.

[51] Uang C.M., Bertero V.V. Evaluation of Seismic Energy in Structures. *Earthquake Engineering and Structural Dynamics*, 19:77–90, 1990.

[52] Earthquake Regulations for Seismic-Isolated Structures : Appendix Chapter 16. *International Conference of Building Officials*, 1997.

[53] United States Geological Survey (USGS) Earthquake Hazards Program. Recent World Earthquakes. *http://earthquake.usgs.gov/recenteqsww/*.

[54] Varadarajan, N. and Nagarajaiah, S. Wind Response Control of Building with Variable Stiffness TMD Using Empirical Mode Decomposition. 130(4):451–458, 2003.

[55] Veletsos A.S. Need for Simple Approaches in Structural Dynamics. In *State of the art in Earthquake Engineering 1981*, pages 258–259, 1980. Prepared for the Occasion of the 7th WCEE in Instanbul, Turkey.

[56] Vision 2000 Committee. Performance Based Seismic Engineering of Buildings. Volume 1 : Interim Recommendations and Conceptual Framework, Structural Engineers Association of California, College Park, MD 20742, April 1995.

[57] Wang, Y. P., and Liu C. J. Active Control of Base-Isolated Structures Under Strong Earthquakes. In *Proceeding of the Fifth USA National Conference on Earthquake Engineering*, volume 1. Chicago, July 10-14.

[58] Wu Z., Soong T. T., Gattulli V., and Lin R. C. Nonlinear Control Algorithms for Peak Response Reduction. Technical Report NCEER-95-0004, National Center for Earthquake Engineering Research, State University of New York at Buffalo, Buffalo, NY. 14261, February 1995.

[59] Xu, Y. L., Qu, W. L., and Ko, J. M. Seismic Response Control of Frame Structures Using MR/ER Dampers. 29:557–575, 2000.

[60] Yoshioka H., Ramallo J. C., and Spencer B. F., Jr. Smart Base Isolation Strategies Employing Magnetorheological Dampers. *Journal of Engineering Mechanics*, 128(5):540–551, 2002.